NASA TECHNICAL NOTE

NASA TN D-2703

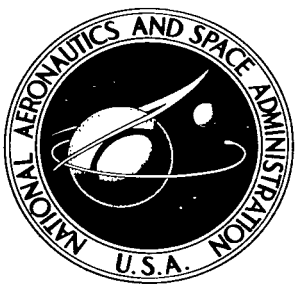

NASA TN D-2703

DESCRIPTION AND INITIAL CALIBRATION OF THE LANGLEY 12-INCH HYPERSONIC CERAMIC-HEATED TUNNEL

by Louis E. Clark

Langley Research Center
Langley Station, Hampton, Va.

NATIONAL AERONAUTICS AND SPACE ADMINISTRATION • WASHINGTON, D. C. • MARCH 1965

DESCRIPTION AND INITIAL CALIBRATION OF THE LANGLEY 12-INCH HYPERSONIC CERAMIC-HEATED TUNNEL

By Louis E. Clark

Langley Research Center
Langley Station, Hampton, Va.

NATIONAL AERONAUTICS AND SPACE ADMINISTRATION

For sale by the Office of Technical Services, Department of Commerce,
Washington, D.C. 20230 -- Price $3.00

DESCRIPTION AND INITIAL CALIBRATION OF THE LANGLEY 12-INCH HYPERSONIC CERAMIC-HEATED TUNNEL

By Louis E. Clark
Langley Research Center

SUMMARY

A description, initial calibration information, and diffuser development are presented for the Langley 12-inch hypersonic ceramic-heated tunnel. This facility is a free-jet wind tunnel utilizing a pebble-bed heat exchanger to provide condensation-free flow at a Mach number of 13.6.

Pitot pressure surveys have shown that the conical nozzle produces a flow satisfactory for many types of testing over a range of stagnation pressure from 60 psia to 615 psia and at stagnation temperatures from 2460° R to 3750° R. The uniform core of the 12-inch-diameter nozzle decreased from 7 inches in diameter at 615 psia to 5.5 inches at 65 psia. The axial Mach number gradient decreased from 0.13 per inch at 615 psia to 0.07 per inch at 80 psia. Total-temperature measurements indicate a maximum total temperature of 3750° R. Total-temperature surveys showed the core of uniform temperature to be smaller than the Mach number core and slightly asymmetric.

The tunnel airstream had a small amount of ceramic-dust contamination which should be insignificant for most tests.

Tunnel pressure recoveries with relatively large models installed decreased from 60 to 65 percent of normal shock recovery to 35 to 45 percent as the stagnation pressure was decreased from 615 psia to 80 psia. The maximum size of the model which could be operated was found to decrease with stagnation pressure from a 5-inch-diameter 60° cone to a 4-inch-diameter 60° cone.

INTRODUCTION

The many new aerodynamic and heat-transfer problems which have accompanied the flight of ballistic missiles, hypersonic gliders, and satellite vehicles at hypersonic speeds and at high altitudes under low Reynolds number conditions have created a need for new types of test facilities. These problems have been investigated at high Mach numbers in helium tunnels (ref. 1), in air at Mach numbers from about 5 to 9 (ref. 2), and in shock tunnels at high Mach numbers and high stagnation temperatures but with very short testing times (ref. 3). Few high Mach number, low Reynolds number tunnels using air and having relatively long test times have been available for studying these problems.

The simulation of flight at high velocities requires high stagnation enthalpies, whereas considerably less enthalpy is needed to avoid the condensation of air which may occur when air is expanded to high Mach numbers. Heat sources have not been available to provide enthalpies which would duplicate flight values at high velocities, but with existing pebble-bed-heater technology sufficient enthalpy can be obtained to avoid the condensation of air at a Mach number of 14. Therefore, a pebble-bed-heated facility (the Langley 12-inch hypersonic ceramic-heated tunnel) was designed to study these new flight problems by providing condensation-free, high Mach number, low Reynolds number simulation. Since the flight enthalpy was not duplicated, the tunnel air velocity was about one-half the flight value and the real-gas effects associated with the flight enthalpy were not simulated. This facility is a blowdown free-jet wind tunnel utilizing a conical nozzle.

When this wind tunnel was designed, many aspects of the operation and performance of tunnel components at the proposed Mach number and Reynolds numbers were generally unknown or were the subject of exploratory investigations. Typical areas in which information was lacking were the range of stagnation conditions over which the conical nozzle would provide satisfactory flow, nozzle boundary-layer growth with Reynolds number, diffuser performance at high Mach numbers and over a range of Reynolds numbers, diffuser blockage characteristics over a range of Reynolds numbers, air liquefaction, and so forth. This report presents a description of the facility, results of a test program to obtain operation and performance characteristics, and initial calibration data.

SYMBOLS

D	diameter
h	heat-transfer coefficient
H_t	total enthalpy
H_w	enthalpy at the wall
l	distance from nozzle throat to exit
M	free-stream Mach number
p_∞	free-stream static pressure
p_e	pressure at diffuser exit
p_c	pressure in free-jet chamber
$p_{t,1}$	total pressure upstream of normal shock

$p_{t,2}$	total pressure behind normal shock
$p_{t,2,CL}$	total pressure behind normal shock on nozzle center line
q	free-stream dynamic pressure
r_n	nozzle throat radius
r_m	model radius
R	free-stream Reynolds number
R_l	free-stream Reynolds number based on distance from nozzle throat to exit
T_∞	free-stream static temperature
T_t	stagnation temperature
$T_{t,CL}$	stagnation temperature on nozzle center line
V	free-stream velocity
x	distance from nozzle exit, positive downstream
δ	boundary-layer thickness
δ^*	boundary-layer displacement thickness
α	nozzle divergence half-angle
λ_2	mean free path behind normal shock
ρ	free-stream density
$\bar{\chi}$	hypersonic viscous-interaction parameter, $\frac{M^3}{\sqrt{R/\text{inch}}}$

DESCRIPTION AND OPERATION OF 12-INCH HYPERSONIC CERAMIC-HEATED TUNNEL

Description of Major Components

The Langley 12-inch hypersonic ceramic-heated tunnel (HCHT) is a blowdown wind tunnel with a free-jet test section. Figure 1 shows the overall layout

and components of the facility including the pebble-bed heater, nozzle, free-jet test section, diffuser, and aftercooler. During a test air enters the pebble-bed heater through the bottom and is heated to the desired stagnation temperature when passing through the pebble bed. The air is then expanded to hypersonic Mach numbers in the conical nozzle and enters the free-jet test section after which it passes through the diffuser and aftercooler into the vacuum sphere.

Figure 2 is a simplified cross-sectional view of the pebble-bed heater. The active portion of the heater is the pebble bed which is 8 inches in diameter and 92 inches long and is made up of 3/8-inch-diameter spherical zirconia pebbles. The bed is contained in a layer of dense zirconia fire brick surrounded by two layers of zirconia insulating brick to reduce heat losses and to maintain the steel heater pressure vessel at safe temperatures. The bed is heated prior to a test by a propane burner located in the flange on the top of the pressure vessel. The products of combustion pass through the bed and are vented to the atmosphere by an exhaust line at the bottom of the heater. The burner uses a mixture of air and propane or air, propane, and oxygen to obtain temperatures up to approximately 4100° F in the top of the pebble bed. Thermocouples located throughout the heater are used to monitor the bed and heater shell during the heating cycle. A quartz window located in the top flange is used with an optical pyrometer to monitor the temperature of the top of the pebble bed during the heating cycle. Water cooling is provided for the burner and several other heater assemblies. It has not been necessary to water cool the pressure vessel since convection and radiation maintain the shell at relatively low temperatures. Equipment is installed which permits the accurate setting of the oxygen, air, and propane flows to the burner. Automatic cutoffs and warning systems are installed to permit continuous operation of the heater without attendants.

Figure 3 shows a simplified cross-sectional view of the nozzle, test section, and diffuser. The nozzle is conical with a total divergence angle of 16°. The nozzle throat diameter is 0.2 inch, the exit diameter is 12 inches, and the distance from throat to exit is 42 inches. The ratio of the nozzle exit area to the throat area is 3600. The nozzle is cooled with a low-pressure water system when the heater is idling or being fired for a test and cooled by a separate high-pressure water system during a test. The free-jet test section can be varied in length up to about 12 inches depending on the diffuser configuration. The chamber surrounding the free-jet test section is constructed of steel and has 10-inch-diameter plate-glass windows of optical quality on the sides for schlieren, shadowgraph, or camera coverage. Models are inserted with a rotary-arm mechanism. Pressure-tube, thermocouple, and electrical connections are provided in the model insertion bay. If desirable, pressure tubing can be run outside the test chamber without excessive lengths, or pressure gages can be located within the model insertion bay. The fixed diffuser is not water cooled and consists of a scoop which captures the free jet, the fixed second minimum, and a subsonic diffuser section. The diffuser is constructed of rolled steel plates and is connected at the exit to an aftercooler composed of a large number of cooling tubes through which water is circulated. The aftercooler cools the air before it enters the 12,000-cubic-foot vacuum sphere and thereby maximum testing time is provided. A valve between the aftercooler and the vacuum sphere isolates these components. A separate line connects the

test chamber to the vacuum pumps (fig. 1) and this line is used when it is necessary to pump the test section independently of the sphere. The present pumping system is capable of evacuating the sphere to 100 microns Hg in about 1 hour after a test.

Operating Method

Since the burner is operated continuously at a heating rate which maintains the top of the pebble bed at approximately 2800° F, the bed can be heated to a maximum temperature of 4100° F for a test in 1 hour. The burner heating rate is increased to a setting which gives the desired temperature, and during the heating period the temperature of the top of the pebble bed is monitored with an optical pyrometer while the temperature of the bottom of the bed is monitored with thermocouples. During the heating period, a conical silicon-rubber plug (fig. 4) is inserted in the nozzle just downstream from the throat and held in place by a rod to prevent products of combustion from entering the test section. This plug seals the nozzle effectively and allows the test section to be pumped as low as 10 microns Hg by the vacuum pump for leak checking, gage calibration, and outgassing of systems prior to a test.

When the desired temperature distribution is established in the bed, the burner is shut off and the heater vessel is prepared for a test by closing all exhaust valves and the combustion air and propane valves and removing the silicon rubber plug from the nozzle. At this time all valves to the heater have been closed, the test section is at atmospheric pressure, and the vacuum sphere has been pumped down to 100 microns Hg. As mentioned previously, the sphere is isolated from the test section by a valve between the aftercooler and sphere. The test section is now pumped to 20 millimeters Hg (by using the separate line to the vacuum pumps) at which time pressurization of the heater is started. The airflow is controlled during pressurization so that the pressure differential across the bed does not exceed 75 percent of the differential pressure required to lift the bed; an automatic pressure switch shuts the air supply valve if this differential pressure is exceeded. During pressurization air flows through the nozzle into the test section and is pumped out through the separate line to the vacuum pump. The vacuum pump maintains the test-section pressure below about 100 millimeters Hg during the 40 seconds required to pressurize the heater vessel to 615 psia. When the desired stagnation pressure is reached, hypersonic flow is established by opening the valve to the sphere which lowers the pressure downstream of the diffuser to the sphere pressure. This method of operation avoids the need for a hot valve upstream of the nozzle to establish the pressure ratio required for hypersonic flow. The hot air which flows through the test section during pressurization does not significantly heat models and instrumentation installed in the model retraction bay. After hypersonic flow is established, the model is inserted with the rotary-arm mechanism. The model is normally retracted before the vacuum sphere reaches the pressure at which flow breakdown occurs. Upon completion of a test the air supply valve is closed and the air in the heater is bled off through a line at the bottom of the heater.

INSTRUMENTS AND CALIBRATION PROCEDURE

Total-Pressure Surveys

The total-pressure surveys were made with the rake shown in figure 5(a), which extended 2 inches across the jet center line. A typical location of the rake with respect to the nozzle exit is shown in figure 3. Rake tubes were constructed in accordance with reference 4 to avoid errors arising from low Reynolds number effects. Strain gage type of pressure gages were used to measure pressures. An electric solenoid operated valve was installed in each rake line between the impact tube and the pressure gage. These valves are closed when the test section is bled to atmospheric pressure to avoid gage zero shift. The valves are also used to improve the time response of the system by setting the pressure in the gage near the anticipated pressure and closing the valves until the rake is inserted into the stream. The rake was left in the stream until flow breakdown which occurred after approximately 50 seconds. Pitot-pressure surveys were made at stagnation pressures of 65, 115, 315, and 615 psia and at stagnation temperatures of 2460° R, 3240° R, and 3750° R. Pressure gages were calibrated before each test by using a McLeod gage as a primary standard with 20 and 50 millimeters Hg dial indicating absolute pressure gages as secondary standards.

Total-Temperature Measurements

The problem of accurately measuring the air stagnation temperature in this low-density hypersonic facility has proved quite difficult and has resulted in the use of several test approaches. In attempting a direct measurement of total temperature, two locations for thermocouple probes were utilized; first, a number of thermocouple probe designs were used for direct measurements in the test section and second, a special probe was designed for measurements in the settling chamber before the flow entered the nozzle. The settling-chamber probe had a water-cooled support section and was inserted into the settling chamber before a test through an access hole in the heater shell which is normally sealed with a water-cooled plug. The probe was located on the center line 4 inches from the nozzle entrance, as shown in figure 2. It was designed to minimize losses due to conduction and radiation and utilized an iridium/iridium-rhodium thermocouple. Total temperatures were measured in the test section by a variety of probes including radiation shielded designs with up to three radiation shields. Two typical total-temperature-probe designs are shown in figures 5(c) and 5(d). Figure 5(c) shows a cold-shield probe in which the thermocouple junction reaches an equilibrium temperature before the shield temperature increases significantly. This probe simplifies the calculation of radiation errors. Figure 5(d) is a typical triple radiation shield probe. The shields are constructed of platinum-rhodium and the probe is designed to permit the inner shield to approach the recovery temperature; thus the radiation correction is eliminated or substantially reduced.

In addition to the measurement of the absolute temperature on the center line, the radial distribution of temperature was determined by use of the rake shown in figure 5(b), which extended 2 inches across the jet center line. The

thermocouple probes on the rake consist of unshielded No. 40 gage platinum-rhodium wires in cross flow supported by No. 24 gage wires. Temperatures in the boundary layer are considered only qualitatively correct. Temperature surveys were made at a stagnation temperature of 3240° R at stagnation pressures of 65, 115, 315, and 615 psia and at stagnation temperatures of 2460° R and 3750° R at a stagnation pressure of 615 psia.

Schlieren Studies

In the low static pressure range of this facility - that is, from 15 to 120 microns Hg - it was expected that the schlieren method would be approaching the limit of its ability. However, studies made with both single- and double-pass systems obtained photographs of the bow shock for relatively large blunt axisymmetric models and relatively clear shocks for two-dimensional models. The double-pass system enabled photographs of bow shocks to be taken at lower stagnation pressures. In general, relatively poor schlieren photographs were obtained and consequently they have not been reproduced in this report.

Free-Jet Chamber Pressure

The pressure in the chamber surrounding the free jet was measured during tests with large blockage models. Thermal conductivity gages with a range of 0 to 1 millimeter Hg were used for these measurements and the gages were calibrated frequently during the tests. The gages were installed directly to the free-jet chamber by the use of quick-connect couplings, and due to the absence of connecting tubing very good time response was obtained.

FACTORS DETERMINING ACCURACY OF CALIBRATION

Vibrational Nonequilibrium Flow

The hypersonic low-density flow which exists in this wind tunnel creates conditions under which thermodynamic nonequilibrium and frozen flow may exist. In the stagnation-temperature range from 2400° R to 3700° R nonequilibrium effects are due to the vibrational degree of freedom inasmuch as these temperatures are not high enough to cause dissociation of air. The rapid expansion of air in the nozzle may cause the vibrational energy mode to deviate from thermodynamic equilibrium.

Values of stream parameters at the test section were calculated for flow frozen at the stagnation chamber and for flow in equilibrium at a stagnation pressure of 615 psia and stagnation temperature of 3600° R ($p_{t,2}/p_{t,1}$ being the same for both flows). Nonequilibrium values fall between these two flow extremes. The results are presented in the following table:

Parameter	Frozen flow	Equilibrium flow
M	13.62	12.93
p_∞, microns Hg	91	100
T_∞, $^\circ$R	95	116
ρ, slug/cu ft	1.57×10^{-6}	1.39×10^{-6}
R, per ft	135,000	111,000
q, lb/sq ft	32.8	33.2
V, ft/sec	6470	6830

The theoretical work of reference 5 shows that the product $\frac{p_{t,1} r_n}{\tan \alpha}$ is a correlating group for vibrational nonequilibrium flow. The values of this product range from 43.6 to 436 lb/in. for the present tests. For these values, reference 5 indicates that the flow properties are very close to the frozen values. The percentage difference between the nonequilibrium values given by reference 5 and frozen-flow values at a stagnation temperature of 3600° R and stagnation pressure of 615 psia is as follows:

M	-2 percent
p_∞	+2 percent
T_∞	+6 percent
ρ	-4 percent
R	-3 percent
q	0 percent
V	+2 percent

The difference between the nonequilibrium values and frozen-flow values would be even smaller at lower stagnation pressures and temperatures. Therefore, in view of the relatively small departure from frozen flow indicated by reference 5 the nozzle has been calibrated by using the ratio $p_{t,2}/p_{t,1}$ and assuming isentropic flow frozen at the stagnation chamber.

Flow-Parameter Errors Due to Pressure-Measurement Inaccuracies

A consideration of the factors affecting the accuracy of the measurement of $p_{t,1}$ and $p_{t,2}$ indicates that the ratio $p_{t,2}/p_{t,1}$ is accurate to within ±4 percent for the most unfavorable case. The errors in the free-stream parameters for a 4-percent error in $p_{t,2}/p_{t,1}$ at a stagnation pressure of 615 psia and a stagnation temperature of 3600° R are as follows:

M	+1 percent
p_∞	-7 percent
T_∞	-1 percent
ρ	-4 percent
R	-5 percent
q	-4 percent
V	0 percent

Flow-Parameter Errors Due to Total-Temperature-Measurement Inaccuracies

The test methods and techniques used to measure total temperature are described in the section entitled "Total-Temperature Measurements" where it is concluded that, if heat loss downstream of the settling-chamber thermocouple probe is negligible, the accuracy of the total-temperature measurement is within ±5 percent. Since the flow is believed to be very close to frozen, the error in total temperature will have a negligible effect on the Mach number, static pressure, and dynamic pressure. The errors in the other free-stream parameters for a ±5-percent error in total temperature are as follows:

T_∞	±5 percent
ρ	±5 percent
R	±7 percent
V	±2.5 percent

Overall Accuracy

Isentropic flow was assumed in the calibration and it is possible that viscous and other effects may cause some degree of nonisentropic flow although this has not been detected. The water vapor produced during the heating cycle by the combustion of propane gas is not believed to have had any significant influence on the data. The heater is purged with supply air with a dewpoint below -85° F during the pressurization process and water-vapor condensation has not been detected in any measurements.

For the most unfavorable case, the deviation of the flow from the frozen condition and the errors in the total-temperature and total-pressure measurements give the following errors in the stream parameters:

M	+1 percent
p_∞	+5 percent
T_∞	-10 percent
ρ	+13 percent
R	+15 percent
q	+4 percent
V	-5 percent

FLOW SURVEYS

Effect of Varying Stagnation Pressure on Nozzle Flow Parameters

Figure 6 shows the variation with stagnation pressure of the ratio $p_{t,2}/p_{t,1}$ and the Mach number on the nozzle center line. As can be noted from the figure, a large boundary-layer growth reduced the Mach number from the frozen inviscid value of 14.87 to 13.62 at 615 psia. As the stagnation pressure was reduced from 615 psia to 65 psia the boundary-layer growth further reduced the Mach number from 13.62 to 12.54 with the most rapid decrease occurring below 300 psia. The data shown were taken during tests spaced over a period of time and repeated in pitot-pressure ratio to within ±4 percent and Mach number to within ±1 percent. For Mach numbers on the order of 30, reference 6 reported a decrease in Mach number with a reduction in pressure, as was found in the present tests, and also reported a change in Mach number with a change in model size and geometry. The variation with model size and geometry was not detected in the present tests for Mach numbers in the range from 11 to 14 except that the free-jet chamber pressure was found to affect the pitot-pressure distribution at the edge of the core for models with large blockage, as is discussed in the section entitled "Tunnel Blockage Characteristics."

Figure 7 presents lateral total-pressure profiles and Mach number distributions for stagnation pressures of 615, 315, 115, and 65 psia at a stagnation temperature of 3240° R. The profiles at all stagnation pressures show the existence of a central core which decreases from 7 inches in diameter at 615 psia to about 5.5 inches at 65 psia. Pitot pressures in the boundary layer are considered only qualitatively correct because of the steep gradients encountered in this region. The variations in pitot pressure and Mach number across the core fall within ±6 percent and ±1.5 percent, respectively. The profile at 65 psia appears to have a slight asymmetry - an increase in pressure to the left edge of the core.

The lateral distribution of total temperature in terms of the fraction of the value at the center line is shown in figure 8(a) for various stagnation pressures at a stagnation temperature of 3240° R. Shown in figure 8(b) is the ratio of pitot pressure at lateral locations to pitot pressure on the center line. The uniform temperature core is not as large as the pitot-pressure core and is asymmetric, with a rapid drop on the right-hand side of the distributions shown. The temperature core does not change significantly with stagnation pressure and a 3-inch core which is centered about 1/2 inch off the nozzle center line has a lateral variation in temperature of 1.5 percent over the range of stagnation pressure.

The axial Mach number gradients for various stagnation pressures are shown in figure 9. A contouring effect of the boundary-layer growth is evident as the gradient decreased from 0.13 per inch at 615 psia to 0.07 per inch at 80 psia.

The average value of the pitot pressure did not change over the 50-second test period for tests over the range of stagnation pressure. Apparently the

diffuser second-minimum section is sufficiently long to prevent the increasing back pressure from feeding through the boundary layer and affecting the test stream.

Effect of Varying Stagnation Temperature on Nozzle Flow Parameters

Figure 10 shows a comparison of $p_{t,2}/p_{t,1}$ on the center line measured at stagnation temperatures of 2460° R and 3750° R with $p_{t,2}/p_{t,1}$ measured at 3240° R for a range of stagnation pressures. The data taken at 2460° R and 3750° R fall within the scatter of the data taken at 3240° R, which indicates that any Reynolds number effect due to the change in stagnation temperature was within the scatter of the data. Lateral pitot-pressure profiles measured at 2460° R and 3750° R also fall within the data scatter of the profiles measured at 3240° R over the range of stagnation pressures.

Surveys to determine the distribution of total temperature taken at 615 psia and stagnation temperatures of 2460° R and 3750° R show the same distribution as those measured at 3240° R shown in figure 8. Total temperature distributions at 2460° R and 3750° R were not measured at other stagnation pressures.

Pitot pressures measured at 2460° R do not show any effect of air condensation; this is in agreement with the experimental results of reference 7 where it was found that condensation was delayed because of an apparent supersaturation. The tunnel operating range is shown in figure 11 taken from reference 7. Also included in the figure are the air saturation curve and the experimentally determined curve for the onset of air condensation in hypersonic wind tunnels. Most of the HCHT operating range lies to the right of the saturation curve for air and consequently well within the region where no condensation has been detected by other investigators. The data taken at 615 psia and 2460° R corresponds to the point shown in the figure at 65° R and 0.091 mm Hg abs. A maximum supersaturation of about 12° R for the present tests occurred at this point. As shown, the condensation point determined by other investigators occurred at a supersaturation of 39° R at this pressure.

Ceramic Dust Contamination of Airstream

Some ceramic-pebble-bed-heated tunnels have suffered from rather severe contamination of the airstream by ceramic dust particles (ref. 8). The HCHT has been found to have only a small amount of dust contamination. Slightly enlarged photographs of a polished $2\frac{1}{2}$-inch-diameter steel hemisphere cylinder before and after 35 seconds of test time give an indication of the dust contamination (see fig. 12). This test was made shortly before the heater was due for yearly maintenance service when dust contamination is most severe. The shiny disks on the model are reflections of the lights used for illumination. Profilometer measurements of the model surface before the test were 3 microinches rms average, whereas measurements taken after the test were from

3 microinches rms average for unpitted surfaces to 25 microinches for the largest pits, with most pits giving a reading from 10 to 15 microinches rms average. As can be seen there are relatively few large pits. This amount of dust contamination will have an insignificant influence for most experiments. The small amount of ceramic particle contamination is attributed to the low flow rate of air through the bed and the side mounting of the nozzle on the heater vessel.

Variation of Boundary-Layer Displacement Thickness and Boundary-Layer Thickness

The variation in boundary-layer displacement thickness at the nozzle exit with stagnation pressure at a stagnation temperature of 3240° R is given in figure 13(a). Displacement thickness was obtained from computation of the area ratio corresponding to the Mach number determined from the ratio $p_{t,2}/p_{t,1}$ at the nozzle exit. The displacement thickness varies from 1.4 inches at 615 psia to 2.15 inches at 65 psia.

Due to the difficulty in theoretically determining the growth of turbulent hypersonic boundary layers, semiempirical formulas have been developed by several investigators to correlate experimental data. Shown in the following table are equations and the conditions under which they have been found to successfully correlate data:

Equations	R_l range	M range	H_w/H_t	Ref.
Boundary-layer displacement thickness				
$\frac{\delta^*}{l} = 0.0463 \frac{M^{1.311}}{R_l^{0.276}}$	10^5 to 10^7	8 to 18	0.1	9
$\frac{\delta^*}{l} = 0.0064 \frac{M^{1.25}}{R_l^{0.14}}$	10^6 to 10^7	9 to 12	≈0.27	10
$\frac{\delta^*}{l} = 1.45 \times 10^{-6} T_t^{0.75} l^{-0.2} p_{t,1}^{-0.333} M^{2.5}$	10^3 to 10^5	11 to 15	≈0.15	11
Boundary-layer thickness				
$\frac{\delta}{l} = 0.066 \frac{M^{0.824}}{R_l^{0.166}}$	10^5 to 10^7	8 to 18	0.1	9

Values of displacement thickness derived by these semiempirical equations are shown in figure 13(a). The equation from reference 9 predicts the thickness very well at 615 psia and predicts slightly greater thicknesses at lower stagnation pressures. The equation from reference 10 gives values in fair agreement with measured values at 615 psia (which represents Reynolds numbers at the low end of the range for which this equation was found to correlate data) but predicts smaller thicknesses at the lower pressures. The equation from reference 11 predicts the trend quite well but gives values about twice the measured values. The equation from reference 11 is not based on experimental data but was found to correlate boundary-layer displacement thicknesses which were computed by the momentum integral method. The nozzles used in these calculations were considerably longer than the nozzle in the present tests.

The variation in boundary-layer thickness at the nozzle exit with stagnation pressure at a stagnation temperature of 3240° R is shown in figure 13(b). The boundary-layer edge was taken as the point where $p_{t,2}$ dropped to 99 percent of the average value across the core. Precise boundary-layer thickness was difficult to determine because of the relatively wide spacing of the survey tubes. The boundary-layer thickness varied from about 2.5 inches at 615 psia to 3.25 inches at 65 psia. Also shown is the boundary-layer thickness predicted by the equation of reference 9. This equation gives fair agreement over the range of pressures, with about a 0.1 inch greater thickness predicted at 615 psia to about a 0.25 inch greater thickness at 65 psia.

TOTAL-TEMPERATURE MEASUREMENTS

Typical results of a series of tests in which temperature measurements were made simultaneously in the settling chamber and in the test section are shown in figure 14. The air total temperature determined from the thermocouple probes is plotted as a function of the temperature of the top of the pebble bed before a test, since the temperature of the top of the bed is used along with other measurements to determine when the bed has been heated sufficiently to provide the desired stagnation temperature. Total-temperature values obtained in the test section were lower than those obtained in the settling chamber. These values differ by about 450° R.

The probe in the settling chamber is located 4 inches from the nozzle entrance as shown in figure 2. The air may lose heat downstream of this point, for example, at the nozzle throat. Measurements in similar nozzles have indicated that the loss of heat in the nozzle is small. It is likely that most of the heat lost in the nozzle would be from the boundary layer and not from the central core. It is, therefore, believed that temperatures indicated by the probe in the settling chamber are the correct values although additional investigation would be required to determine definitely that heat loss downstream of the probe is negligible.

The measurements taken with the probe in the settling chamber with the assumption that heat loss in the nozzle is negligible are considered to be accurate to within ±5 percent. On this basis an extrapolation of the

settling-chamber data shown in figure 14 indicates a maximum total temperature of 3750° R. If there is heat loss downstream of the settling chamber, the air temperature would fall between the settling-chamber and test-section data.

TUNNEL BLOCKAGE CHARACTERISTICS

Model Capability

The performance of the final diffuser for typical models over the range of stagnation conditions is summarized in figure 15. The relative performance of three diffuser configurations, tested to obtain the desired compromise between model capability and testing time, is given in the appendix. Figure 15 shows the reduction in the maximum size of cone, hemisphere, and flat-face models which can be operated and the reduction in diffuser pressure recovery with the model in the airstream as the stagnation pressure is decreased. The flagged symbols in the figure indicate the lowest pressure at which the model could be operated (tests were usually made at 100 psi increments). At lower stagnation pressures the model could not be operated with any efficiency even when large pressure ratios were available.

At stagnation pressures from 500 to 615 psia the tunnel would operate with hemisphere models up to 4 inches in diameter, 60° cone models up to 5 inches in diameter, and flat-face models up to 3 inches in diameter. The 5-inch-diameter 60° cone corresponds to a blockage area (including strut) of 19 percent of the nozzle exit area and 55 percent of the isentropic core area at 615 psia. The pressure recovery for these models varied from 55 percent of normal shock recovery for the flat-face model to 60 percent for the 60° cone model.

As shown in figure 15 the maximum size model of any geometry which could be operated decreased with a reduction in stagnation pressure. A typical example is the 60° cone models. The 5-inch-diameter 60° cone could be operated from 600 to 515 psia, whereas the 4-inch-diameter 60° cone could be operated from 600 to 135 psia. In general, pressure recoveries for the relatively large models tested decreased from 60 to 65 percent of normal shock recovery at 615 psia to 35 to 45 percent at 80 psia as compared with clear-tunnel pressure recovery which varied from 80 percent of normal shock recovery at 600 psia to 55 percent at 65 psia.

It was found that larger models could be tested by starting the flow and inserting the model rather than by attempting to start the tunnel with the model in the test section. The 4-inch-diameter hemisphere was marginal at 500 psia. At this pressure the model might block the flow on the first insertion but frequently the tunnel could be operated by removing and reinserting the model.

Effect of Free-Jet Chamber Pressure on Lateral Pitot-Pressure Distribution

The operation of large blockage models in the HCHT results in increases of the pressure in the chamber surrounding the free jet of up to four times the free-stream static pressure. Since the nozzle is operated in an over-expanded condition, a reversed conical shock is assumed to emanate from the region of the nozzle lip and trail downstream. This shock system supports the pressure difference between the free-jet chamber and the free stream. An increase in chamber pressure requires a stronger shock system to support the pressure difference. This shock is inclined at a greater angle to the stream and tends to move toward the stream center line where it may affect the pitot-pressure distribution.

A series of tests of the effect of chamber pressure on lateral pitot-pressure profiles were made with a flat disk normal to the flow mounted some distance behind the pitot-pressure survey rake. Disks of various sizes were used to produce the desired changes in free-jet chamber pressure. Figure 16 shows the effect of various levels of free-jet chamber pressure on the lateral pitot-pressure distribution for a typical diffuser configuration. As the chamber pressure is increased the pitot pressure at the edge of the core increases until at a chamber pressure of 410 microns Hg an apparent increase in the uniform core has occurred, but this is actually nonisentropic flow caused by the presence of the shock system. Further increases in chamber pressure cause the pitot pressure at the edge of the core to increase to $1\frac{1}{2}$ times the center line value.

Figure 17 shows the results of a series of tests made with the final diffuser configuration over the range of stagnation pressure at high chamber pressures typical of large blockage models. Chamber pressures up to four times free-stream static pressure did not affect the uniform core at stagnation pressures from 615 to 65 psia. At 115 psia the region of increased pitot pressure was not detected. Since the shock moves from the position 4 inches off the center line at 315 psia to 3 inches off the center line at 65 psia, it is probable that the shock is between these stations at 115 psia.

These tests furnish some insight into the operation of the free jet and provide a basis for estimating the model size at which adverse flow effects due to the effect of free-jet chamber pressure on the shock system may occur. Since the largest axisymmetric models which can be operated at each stagnation pressure will not be in the region of increased pitot pressure, it does not appear that this effect will influence model testing except for long, large, blunt models which may be affected by shock intersections on the afterbody.

However, the large blockage models may be unsuitable for obtaining afterbody pressure and heat-transfer data since it has been determined in other free jets at Langley that this type of data may be questionable when obtained with models close to the blockage limits of the tunnel even when the model is not in the region affected by the shock system. It is believed that this effect is

possibly due to a pressure feedback through the wake from the high-pressure region in the diffuser entrance.

FLIGHT REGIMES SIMULATED

Simulation of flight at high altitude requires duplication of the appropriate low-density simulation parameter as well as the conventional similarity parameters of Mach number and Reynolds number. Reference 12 has delineated low-density hypersonic flight regimes for axisymmetric blunt bodies in terms of the mean free path and nose radius. Flight regimes simulated by the HCHT are from the boundary-layer regime to the fully merged layer (fig. 18). The characteristic length used in this figure was the radius of hemisphere cylinders which can be operated satisfactorily in the tunnel (0.2 inch to 1.75 inches).

A comparison of the chemical kinetic regime with the rarefied gas regimes of reference 12 for a nose radius of 1 foot is presented in figure 19 which is from reference 13. The HCHT provides Mach number simulation for bodies traveling at 10,000 to 12,000 feet per second and it can be seen from figures 18 and 19 that most of the flight regimes simulated by this facility fall in the region where chemical effects are negligible (defined as either (1) air temperatures are not high enough to produce dissociation or (2) time is not available for any appreciable reaction to occur and flow is essentially frozen at the atmospheric composition). In this region viscous effects predominate, and it has been pointed out by reference 13 that energy density need not be reproduced since time is not available for an appreciable reaction to occur and aerodynamic and heat-transfer characteristics can be established by Reynolds number, Mach number, and low-density parameter simulation. In general, the HCHT can provide simulation of Mach number and one other parameter and in some instances can provide simulation of all three parameters. Each investigation will require individual consideration. Figure 20 showing the range of tunnel parameters is included as an aid in determining whether the tunnel is suitable for a particular investigation.

CONCLUDING REMARKS

An experimental program has been conducted to obtain operation and performance characteristics and calibration data for a 12-inch hypersonic ceramic-heated open-jet wind tunnel at the Langley Research Center. Results of this program indicated that the following remarks should be emphasized:

The flow produced by the conical nozzle over a range of stagnation pressure from 615 to 65 psia and stagnation temperature from 2460° R to 3750° R appears suitable for many types of tests. The conical nozzle produced a flow with a lateral variation in Mach number of ±1.5 percent and an axial Mach number gradient decreasing from 0.13 per inch at 615 psia to 0.07 per inch at 80 psia.

The boundary layer decreased the Mach number from the inviscid value of 14.87 to between 13.62 and 12.54 depending upon stagnation pressure. The uniform core of the 12-inch-diameter nozzle varied in size from 7 inches in diameter at 615 psia to 5.5 inches at 65 psia. Boundary-layer displacement thicknesses and boundary-layer thicknesses determined over a range of stagnation conditions were in approximate agreement with the empirical relationship developed in U.S. Air Force ASD Technical Report 61-645.

For the final diffuser system a 5-inch-diameter 60° cone model with a blockage area of 19 percent of the nozzle exit area and 55 percent of the isentropic core area could be operated at 600 psia with a diffuser pressure recovery of 60 percent of normal shock recovery as compared with a clear-tunnel pressure recovery of 80 percent. The maximum size model which could be operated decreased with a reduction in stagnation pressure. At 115 psia the largest 60° cone which could be operated was 4 inches in diameter. In general, pressure recoveries for relatively large models decreased from 60 to 65 percent of normal shock recovery at 615 psia to 35 to 45 percent at 80 psia.

Total-temperature measurements taken upstream of the nozzle entrance indicate a maximum total temperature attained with the ceramic heat exchanger to be about 3750° R. A 3-inch core centered about 1/2 inch off the nozzle center line has a lateral variation in temperature of ±1.5 percent.

A small amount of ceramic-dust contamination was found in the airstream. This amount of contamination will have an insignificant influence for most tests.

In the chamber surrounding the free jet, high pressures due to large blockage models influenced the lateral Mach number distribution. However, free-jet chamber pressures as high as four times free-stream static pressure did not affect the uniform core over the range of stagnation pressures.

Langley Research Center,
National Aeronautics and Space Administration,
Langley Station, Hampton, Va., December 2, 1964.

APPENDIX

COMPARISON OF THREE FIXED DIFFUSER CONFIGURATIONS AT MACH NUMBERS IN THE VICINITY OF 13 AND AT REYNOLDS NUMBERS FROM 17,000 TO 160,000 PER FOOT

The diffuser of a hypersonic wind tunnel determines the pressure ratio required to start and maintain hypersonic flow; therefore, in an intermittent wind tunnel such as the Langley 12-inch hypersonic ceramic-heated tunnel the diffuser determines the available operating time. Diffusers may be either of the fixed or adjustable type. In the adjustable-type diffuser the hypersonic flow is started with a relatively large diffuser throat area which is then reduced to provide the optimum operation time. In the fixed-type diffuser a compromise diffuser throat area must be determined which is large enough to prevent blockage and yet efficient enough to provide reasonable operation time for models. Because of significant viscous losses which occur at high Mach numbers and low Reynolds number conditions and the interference effect of the model, diffuser performance has been difficult to predict theoretically and experiment has been relied upon in diffuser design. The present tests were limited to the three fixed diffuser configurations which were required to evolve a diffuser configuration that would provide a satisfactory compromise between the ability to operate with large models and tunnel operating time. Tests were also made to determine the clear-tunnel pressure recovery over a range of Reynolds number for the three configurations.

Although limited, these tests at Mach numbers from 12.5 to 13.6 and free-stream Reynolds numbers per foot from 17,000 to 160,000 provide the designer with needed information at high Mach numbers and at Reynolds numbers from the lowest of 2,670 per foot reported by references 14 and 15 to those from 100,000 to 200,000 per foot reported in references 16, 17, and 18.

Test Procedure

During these tests the minimum pressure ratio for maintaining flow was measured for the diffuser configurations with and without models in the air-stream. Models were tested at a constant stagnation pressure until the vacuum sphere reached a pressure at which flow breakdown occurred. The pressure at the diffuser exit at this time was taken to be the diffuser pressure recovery. Flow breakdown was determined by the sudden increase in the model pitot pressure and the simultaneous increase in the pressure in the chamber surrounding the free jet. Clear-tunnel pressure recovery was determined in a similar manner. Although detailed measurements were not made, starting pressure ratios were determined to be approximately the same as operating pressure ratios except at the lower stagnation pressures where greater starting pressure ratios were required.

APPENDIX

Diffuser pressure recoveries have been expressed in terms of the percent of test-section pitot pressure at the model location recovered by the diffuser. Diffuser performance expressed in this manner will be 100 percent when the diffuser pressure recovery equals the test-section pitot pressure (referred to as normal shock recovery). When a positive axial Mach number gradient exists as in the present tests, the pitot pressure will decrease with distance from the nozzle exit. The data reported herein are considered to be conservative since the pitot pressure used to determine the diffuser performance was taken at a typical model location 2.3 inches from the nozzle exit.

Model Capability of Diffuser Configurations

The three diffuser configurations tested in this investigation to obtain a diffuser which would provide a satisfactory compromise between tunnel operation with reasonably large models and testing time are shown in figure 21. Because of a lack of design data for diffusers in these Mach number and Reynolds number ranges, basic diffuser design was based on data from reference 19 which gives results of an investigation with diffusers at Mach 6 and Reynolds numbers per foot of 10^6. The following table summarizes the model capability and operating time of the three diffuser configurations at a stagnation pressure of 615 psia and a stagnation temperature of 3240° R:

Configuration	Flow maintained	Test time, sec	Flow lost	Clear-tunnel operating time, sec
1	2.5-in. D hemisphere cylinder	48	3.0-in. D hemisphere cylinder	65
2	3.0-in. D hemisphere cylinder	48	4.0-in. D hemisphere cylinder	65
3	4.0-in. D hemisphere cylinder	25	4.5-in. D hemisphere cylinder	57

The design of diffuser configuration 1, the initial configuration, was based on the data of reference 19 and a 15° entrance scoop was chosen to permit the longest free-jet length consistent with the size of the free-jet chamber. With this configuration the tunnel could be operated with hemisphere models up to 2.5 inches in diameter. Reference 19 indicated that changing the scoop of configuration 1 from a 15° scoop to a two-stage (two angle) 15°-8° scoop and shortening the free-jet length would improve model capability. Diffuser configuration 2, the two-stage-scoop configuration, made possible operation of the tunnel with hemisphere models up to 3 inches in diameter. In an effort to further increase the model capability, the throat area of configuration 2 was increased from 69 percent to 79 percent of the nozzle exit area. Configuration 3, with the increased throat area, allowed the tunnel to operate

with hemisphere models up to 4 inches in diameter, but the operating time for the clear tunnel and a 3-inch-diameter hemisphere model decreased about 10 percent. The 4-inch-diameter hemisphere met the requirements of the test program and, therefore, only these three configurations were tested.

Variation in Diffuser Performance With Reynolds Number

Measurements were made to determine the performance of the three diffuser configurations over a range of Reynolds numbers. To obtain the Reynolds number variation, tests were conducted at a constant stagnation temperature over a range of stagnation pressure. Figure 22 shows the percentage variation of normal shock pressure recovery for the clear tunnel with Reynolds number per foot and the corresponding stagnation pressure. Over this range of Reynolds number all configurations had decreases in pressure recovery, but the relative performance of the diffuser configurations remained the same. Configurations 1 and 2 had the same clear-tunnel performance over the range of Reynolds number with a decrease from 90 percent at a Reynolds number of 160,000 $\left(p_{t,1} = 600 \text{ psia}\right)$ to 60 percent at a Reynolds number of 17,000 per foot $\left(p_{t,1} = 60 \text{ psia}\right)$, whereas configuration 3 was about 10 percent lower over this range. Figure 23 shows these data in terms of the pressure ratio required to maintain flow. Configurations 1 and 2 required a pressure ratio of 1600 and configuration 3 required a pressure ratio of 1800 over the range of Reynolds number and stagnation pressure. This method of presentation also indicates a decrease in diffuser performance at lower Reynolds numbers since a reduction in pressure ratio would be expected with the decrease in Mach number with Reynolds number. The constant pressure ratio may be the result of compensating trends with the expected decrease in pressure ratio with a decrease in Mach number being offset by the greater viscous effects at Lower Reynolds numbers. The clear-tunnel operating time remained about constant over the range of Reynolds number, which would be expected as a result of the constant pressure ratio required to maintain flow over this range. It was also determined that all diffusers had decreases of 20 to 25 percent in pressure recovery with large models installed over this range of Reynolds number and that the relative performance of the diffusers with models did not change over this range.

Comparison With Other Free-Jet Wind Tunnels

Figure 24 shows a comparison of the clear-tunnel pressure recovery for the Langley 12-inch hypersonic ceramic-heated tunnel with other free-jet wind tunnels in the Mach number range from 6 to 20. The data have been selected as nearly as possible to eliminate geometrical differences, Reynolds number effects, test-section location on which diffuser recovery is based, and so forth, and it is believed that these factors will have a relatively small effect on the comparison. Within these limitations it appears that Mach number has a moderate effect on normal-shock pressure recovery. For an area ratio of 0.6, recoveries for the clear tunnel of about 36 percent greater than normal shock are obtained at a Mach number of 6, whereas recoveries close to 100 percent of normal shock recovery can be obtained at Mach numbers from 12 to 19.

APPENDIX

Figure 25 shows a comparison of the clear-tunnel pressure recovery of the HCHT with other free-jet wind tunnels over a range of free-stream Reynolds number per foot. Geometrical differences between these tunnels other than the second minimum area ratio are believed to have a small influence on the comparison. The second minimum area ratio for each tunnel is shown below the data point corresponding to that tunnel. With the exception of the Mach 6 data at a Reynolds number of 10^6, all data points are for Mach numbers greater than about 10 where the effect of Mach number appears to be small. The data at Mach 6 are included since this diffuser was of almost identical geometry as the diffuser in the present tests. Considering the Mach number difference between the tests, it is seen that general agreement is obtained between the Mach 6 data and an extrapolation of the data from the present tests to a Reynolds number of 10^6. The data for an area ratio of 1 were obtained from reference 18 by basing the pressure recovery on measurements made at a station 2 inches from the nozzle exit at which point the local Mach number was approximately the same as that of the present tests, and these data are in general agreement with the HCHT data. The Ohio State and ARL data are also in general agreement with data of the present tests. The trend of the data from the present tests is to approach the results obtained at AEDC at a Reynolds number per foot of 2,670, and an extrapolation of the 0.69 area-ratio data of the present tests is in general agreement with the 0.68 area-ratio data from AEDC. The most efficient area ratio was found to be 1 by AEDC, whereas it was at least as low as 0.69 in the present tests and as low at 0.6 in the tests of reference 19. It appears that a curve showing the variation of normal shock pressure recovery with Reynolds number for an area ratio of 1 must cross over the curves for area ratios of 0.69 and 0.79 at Reynolds numbers per foot between 17,000 and 2,670 as the larger area ratio becomes more efficient.

Figure 25 illustrates the general trend of decreasing diffuser pressure recovery from values in excess of normal shock recovery at Reynolds numbers of 10^6 to 10 to 20 percent of normal shock recovery for a Reynolds number of 2,670 per foot. At the higher Reynolds numbers the highest clear-tunnel performance is for a diffuser second minimum area ratio of 0.6 or lower, whereas at Reynolds numbers between 17,000 and 2,670 the performance is more efficient for an area ratio of 1.0. However, it should be pointed out that the configuration which provides the highest clear-tunnel performance may not provide the optimum compromise in terms of models which can be operated.

REFERENCES

1. Mueller, James N.; Close, William H.; and Henderson, Arthur, Jr.: An Investigation of Induced-Pressure Phenomena on Axially Symmetric, Flow-Alined, Cylindrical Models Equipped With Different Nose Shapes at Free-Stream Mach Numbers From 15.6 to 21 in Helium. NASA TN D-373, May 1960.

2. Bertram, Mitchel H.: Boundary-Layer Displacement Effects in Air at Mach Numbers of 6.8 and 9.6. NASA TR R-22, 1959. (Supersedes NACA TN 4133.)

3. Cheng, H. K.; Hall, J. Gordon; Golian, T. C.; and Hertzberg, A.: Boundary-Layer Displacement and Leading-Edge Bluntness Effects in High-Temperature Hypersonic Flow. J. Aerospace Sci., vol. 28, no. 5, May 1961, pp. 353-381, 410.

4. Bailey, A. B.; and Boylan, D. E.: Some Experiments on Impact-Pressure Probes in a Low-Density, Hypervelocity Flow. AEDC-TN-61-161 (Contract No. AF 40(600)-800 S/A 24(61-73), Arnold Eng. Develop. Center, Dec. 1961.

5. Stollery, J. L.; and Park, C.: Computor Solutions to the Problem of Vibrational Relaxation in Hypersonic Nozzle Flows. Rep. No. 115, Aeron. Dept., Imp. Coll. Sci. Technol., Jan. 1963.

6. Johnson, Robert H.: Hypersonic Viscous Effects in Wind Tunnels. ARS Jour., (Tech Notes), vol. 31, no. 7, July 1961, pp. 1022-1024.

7. Daum, Fred L.: Air Condensation in a Hypersonic Wind Tunnel. AIAA Jour., vol. 1, no. 5, May 1963, pp. 1043-1046.

8. Trout, Otto F., Jr.: Design, Operation, and Testing Capabilities of the Langley 11-Inch Ceramic-Heated Tunnel. NASA TN D-1598, 1963.

9. Burke, Andrew F.: Turbulent Boundary Layers on Highly Cooled Surfaces at High Mach Numbers. Proceedings of Symposium on Aerothermoelasticity. ASD Tech. Rept. 61-645, U.S. Air Force, 1961, pp. 704-741.

10. Lee, John D.: Axisymmetric Nozzles for Hypersonic Flows. Rept. No. TN(ALOSU) 459-1 (WADC TN 59-228), Ohio State Univ. Res. Found., June 1959.

11. Enkenhus, K. R.; and Maher, E. F.: The Aerodynamic Design of Axisymmetric Nozzles for High-Temperature Air. NAVWEPS Rep. 7395, U.S. Naval Ord. Lab. (White Oak, Md.), Feb. 5, 1962.

12. Probstein, Ronald F.: Shock Wave and Flow Field Development in Hypersonic Re-Entry. ARS J., vol. 31, no. 2, Feb. 1961, pp. 185-194.

13. Harney, Donald J.: Chemical Kinetic Regimes of Hypersonic Flight Simulation. AEDC-TDR-63-3, U.S. Air Force, Jan. 1963.

14. Potter, J. Leith; Kinslow, Max; Arney, George D., Jr.; and Bailey, Allan B.: Description and Preliminary Calibration of a Low-Density, Hypervelocity Wind Tunnel. AEDC-TN-61-83, U.S. Air Force, Aug. 1961.

15. Milligan, M. W.; and Bailey, J. F.: Low-Density Hypervelocity Wind Tunnel Diffuser Performance. AEDC-TDR-63-30, U.S. Air Force, Jan. 1963.

16. Thomas, R. E.; Lee, J. D.; and Von Eschen, G. L.: Configuration Details and Initial Performance of a Hypersonic Wind Tunnel for the Range of Mach Number 8 to 14. Tech. Rept. No. 2 (Contract DA-33-019-ORD-1634), Ohio State Univ. Res. Found., Oct. 1957.

17. Thomas, R. E.; and Lee, J. D.: The Ohio State University 12-Inch Hypersonic Wind Tunnel System. Rep. No. TN(ALOSU)559-2 (WADC TN 59-280), Ohio State Univ. Res. Foundation, July 1959.

18. Gowen, Forrest E.; and Hopkins, Vaughn D.: A Wind Tunnel Using Arc-Heated Air For Mach Numbers From 10 to 20. Advances in Hypervelocity Techniques, Arthur M. Krill, ed., Plenum Press, 1962, pp. 27-46.

19. Midden, Raymond E.; and Cocke, Bennie W., Jr.: Diffuser Performance of a Mach 6 Open-Jet Tunnel and Model-Blockage Effects at Stagnation Temperatures to 3,600° F. NASA TN D-2384, July 1964.

20. Scaggs, N. E.; Burggraf, W.; and Gregorek, G. M.: The ARL Thirty-Inch Hypersonic Wind Tunnel Initial Calibration and Performance. ARL 63-223, U.S. Air Force, Dec. 1963.

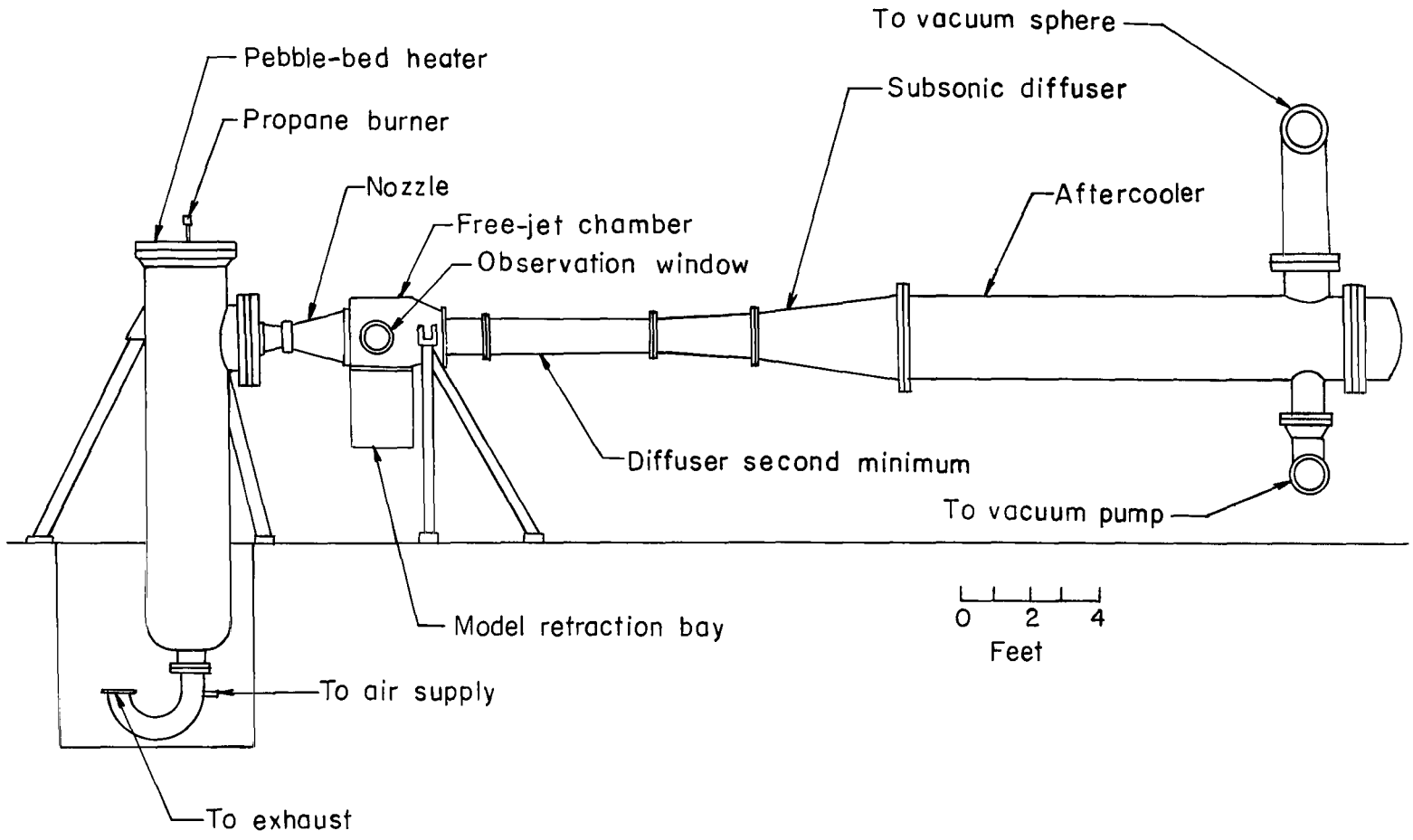

Figure 1.- Schematic drawing of 12-inch hypersonic ceramic-heated tunnel.

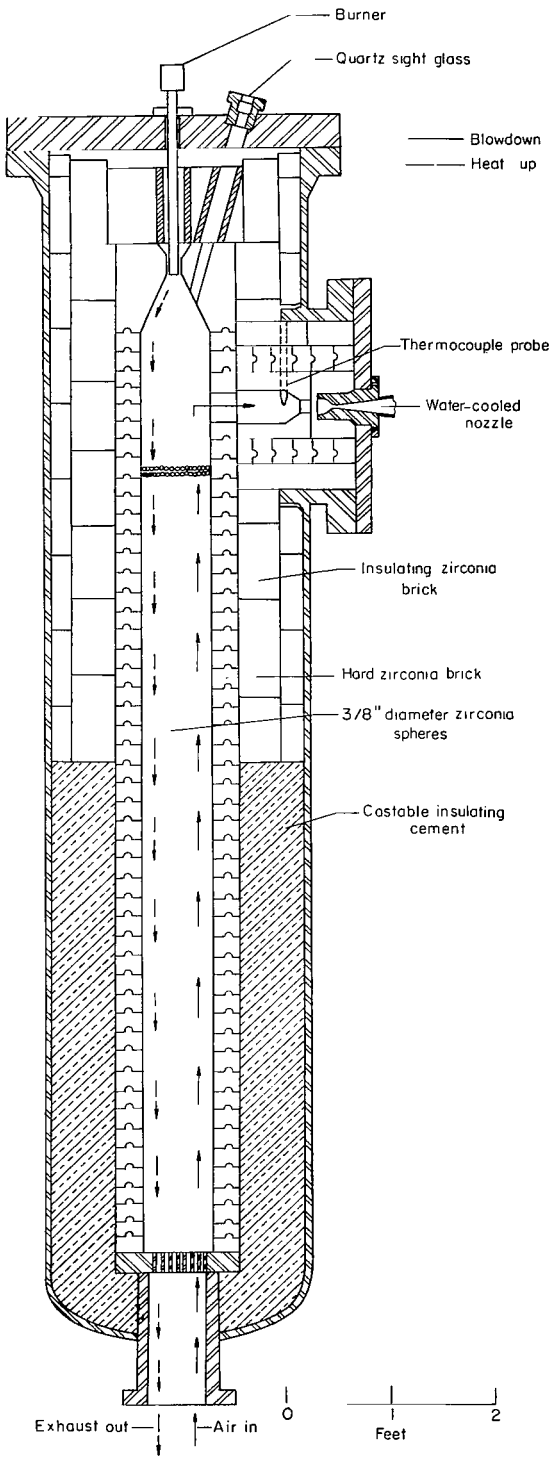

Figure 2.- Cross-sectional view of pebble-bed heater.

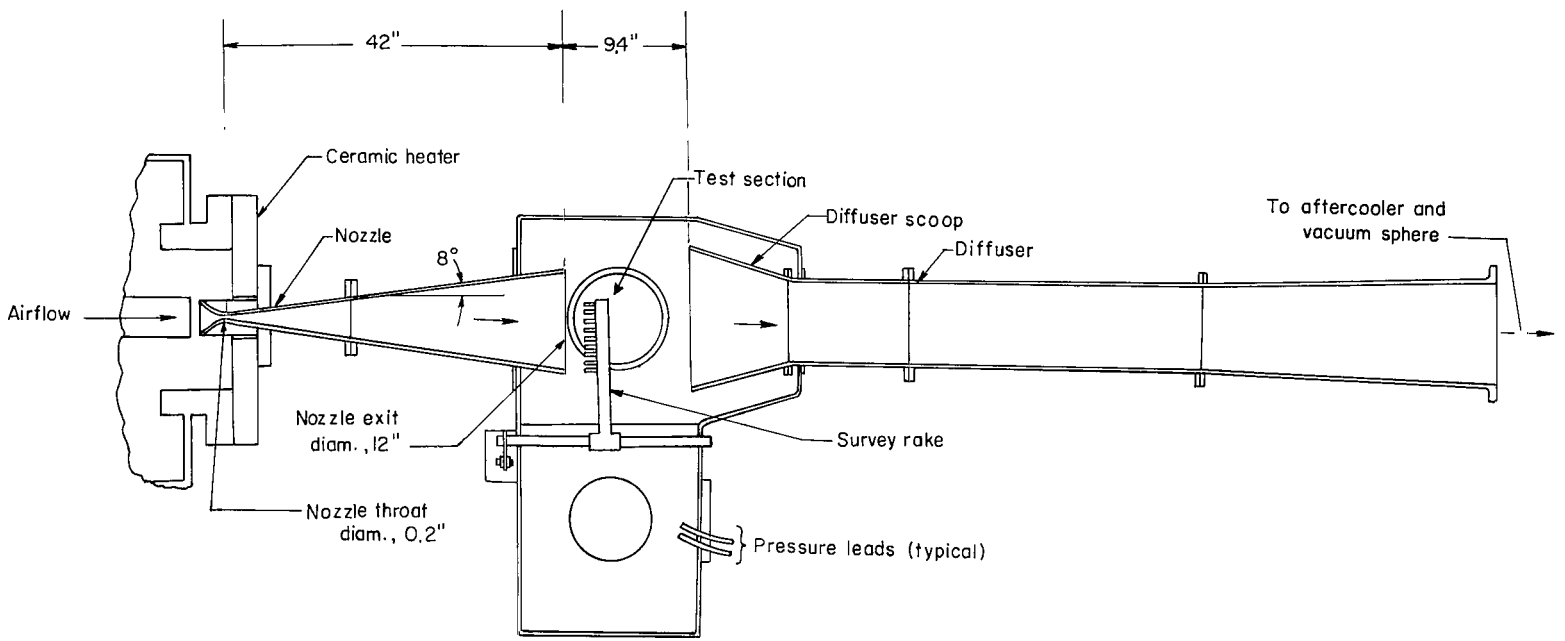

Figure 3.- Cross-sectional view of nozzle, test section, and diffuser.

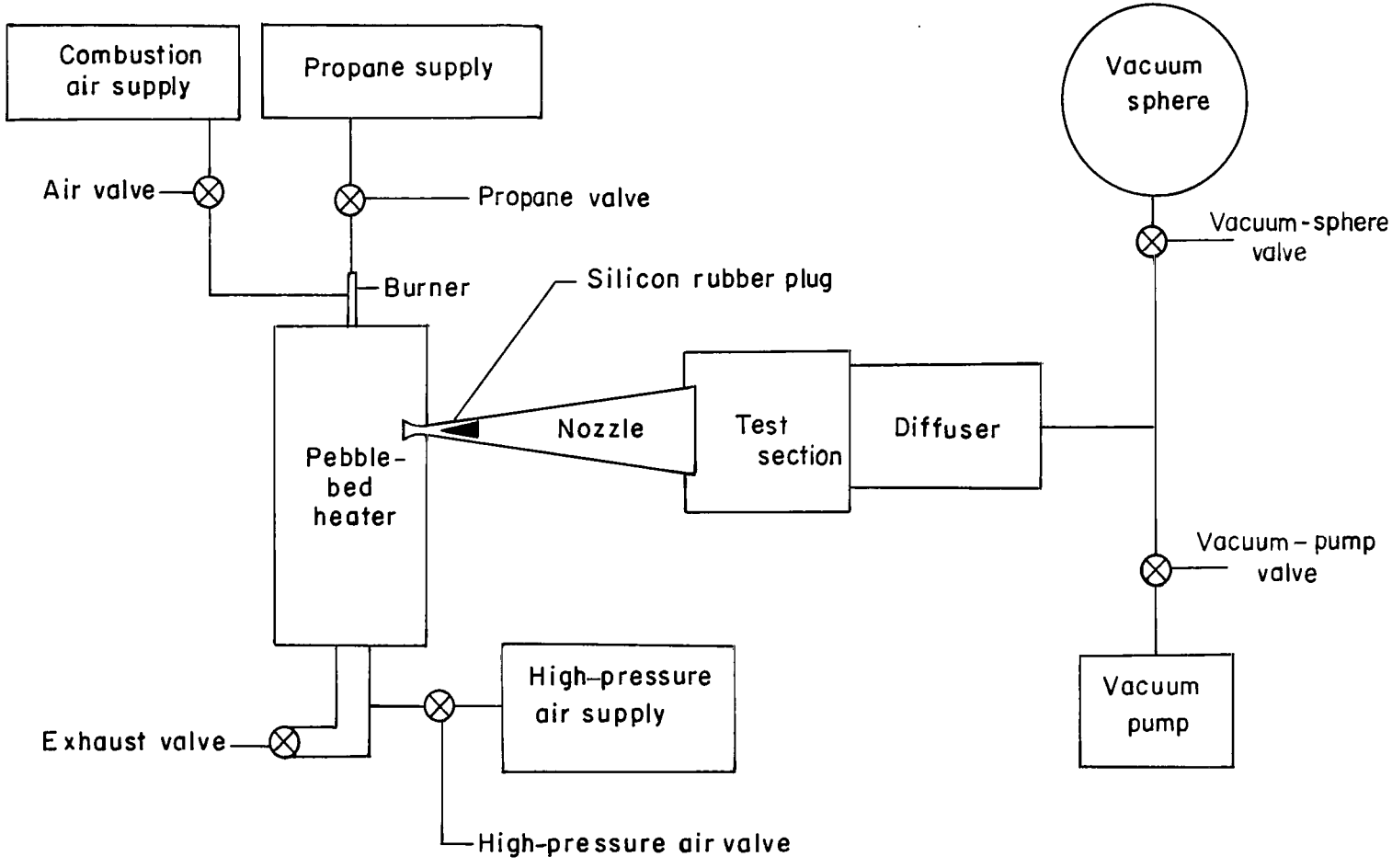

Figure 4.- Block diagram of Langley 12-inch hypersonic ceramic-heated tunnel.

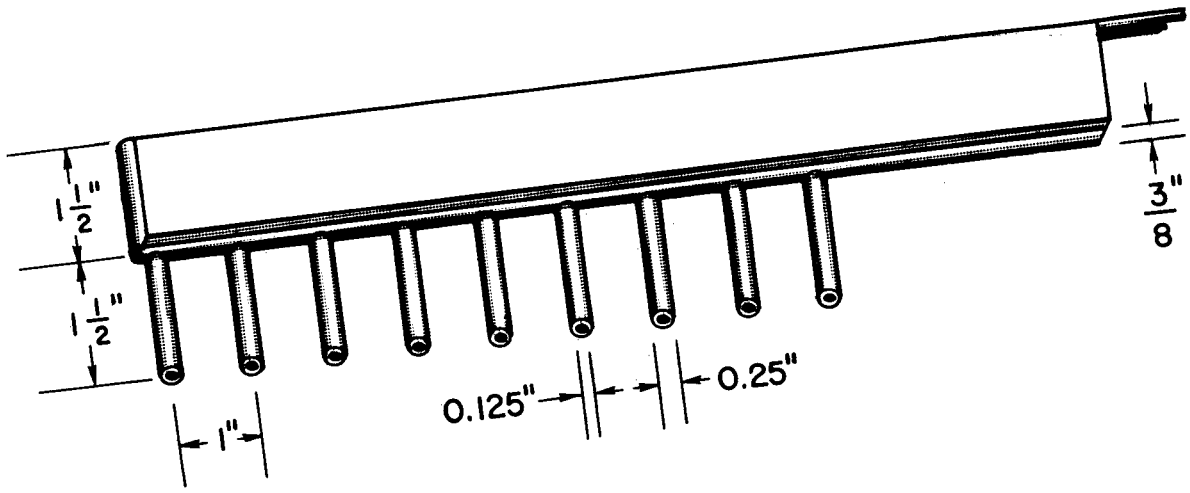

(a) Total-pressure survey rake.

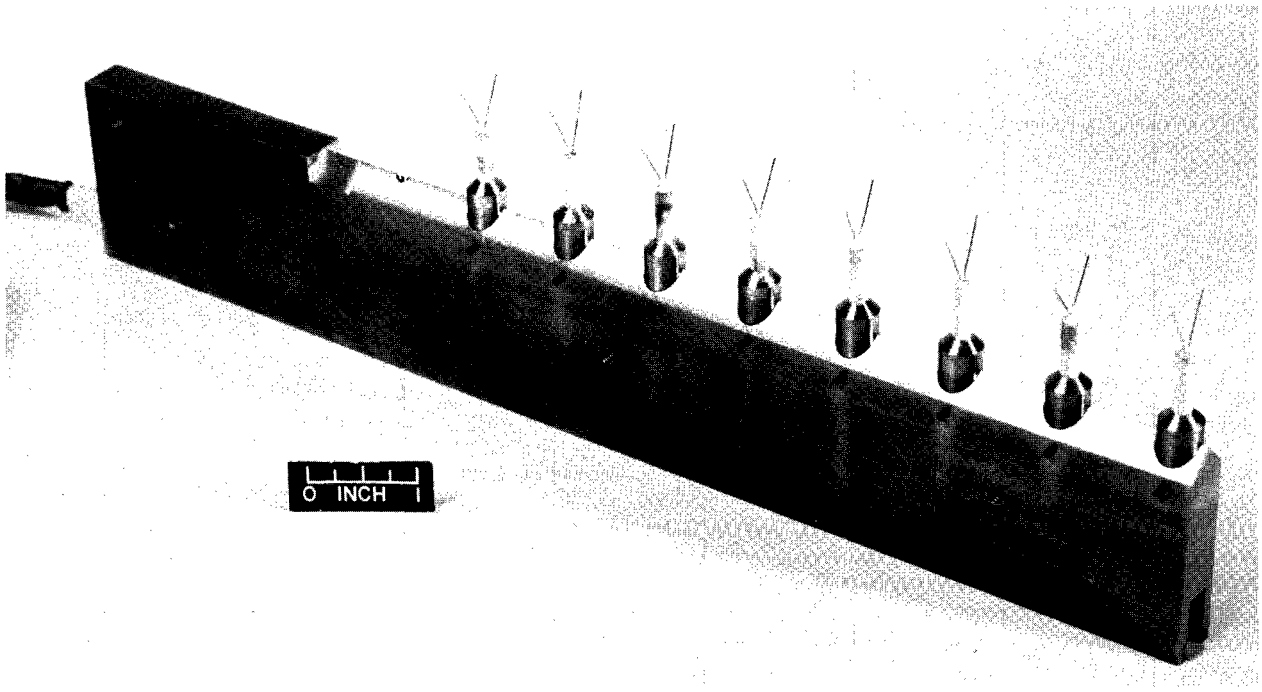

(b) Total-temperature survey rake. L-63-6934

Figure 5.- Instruments used in measuring pressure and temperature in Langley 12-inch ceramic-heated tunnel.

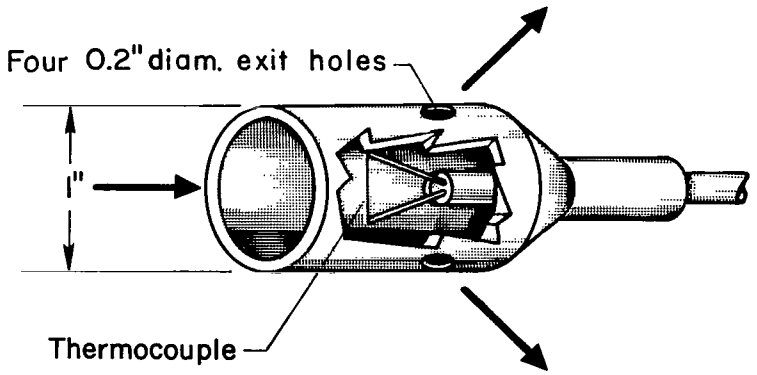

(c) Cold-shield temperature probe.

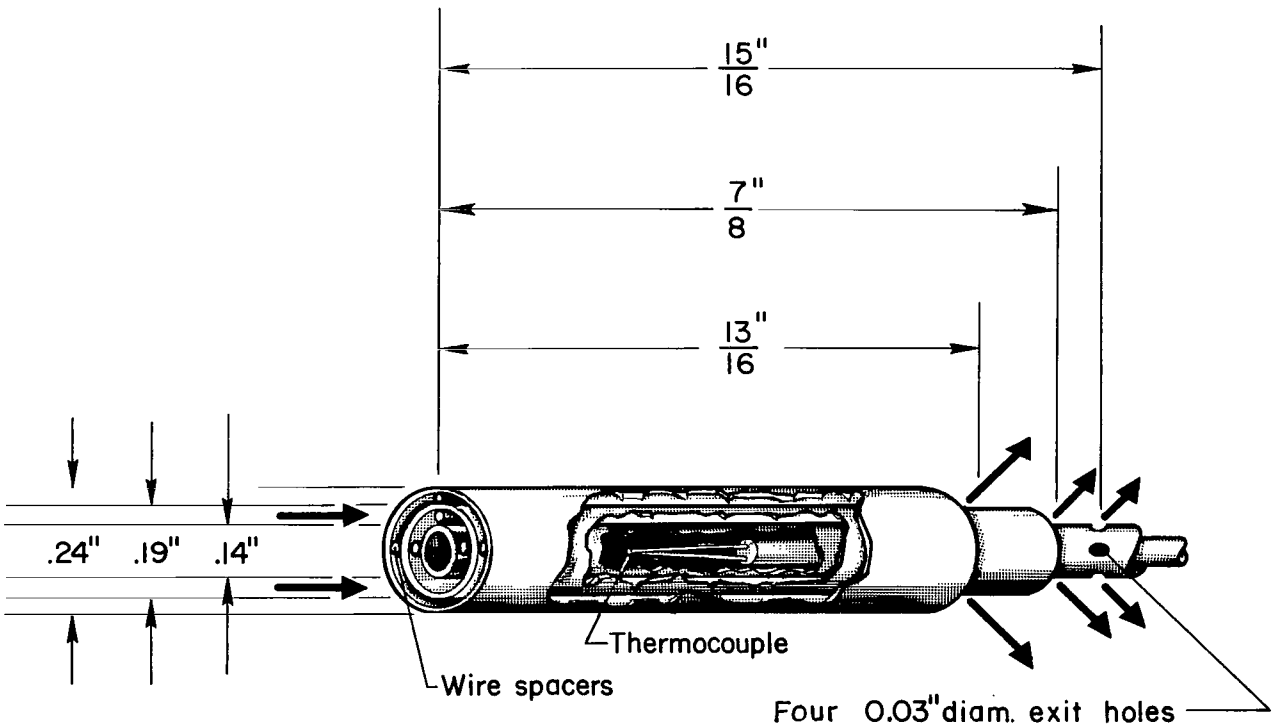

(d) Triple-shield temperature probe.

Figure 5.- Concluded.

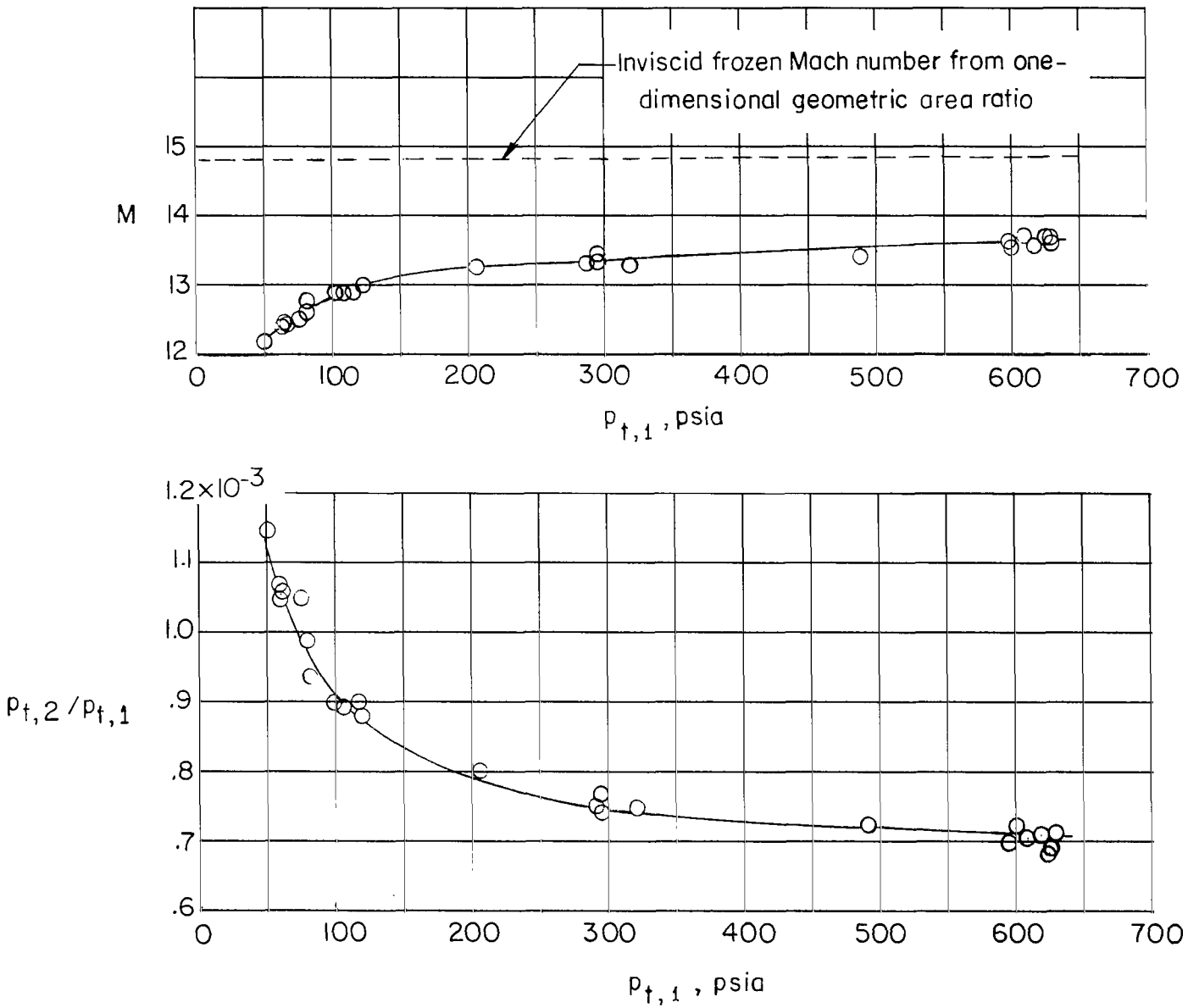

Figure 6.- Variation of $p_{t,2}/p_{t,1}$ and M on center line with stagnation pressure at x = 2.3 inches. T_t = 3240° R.

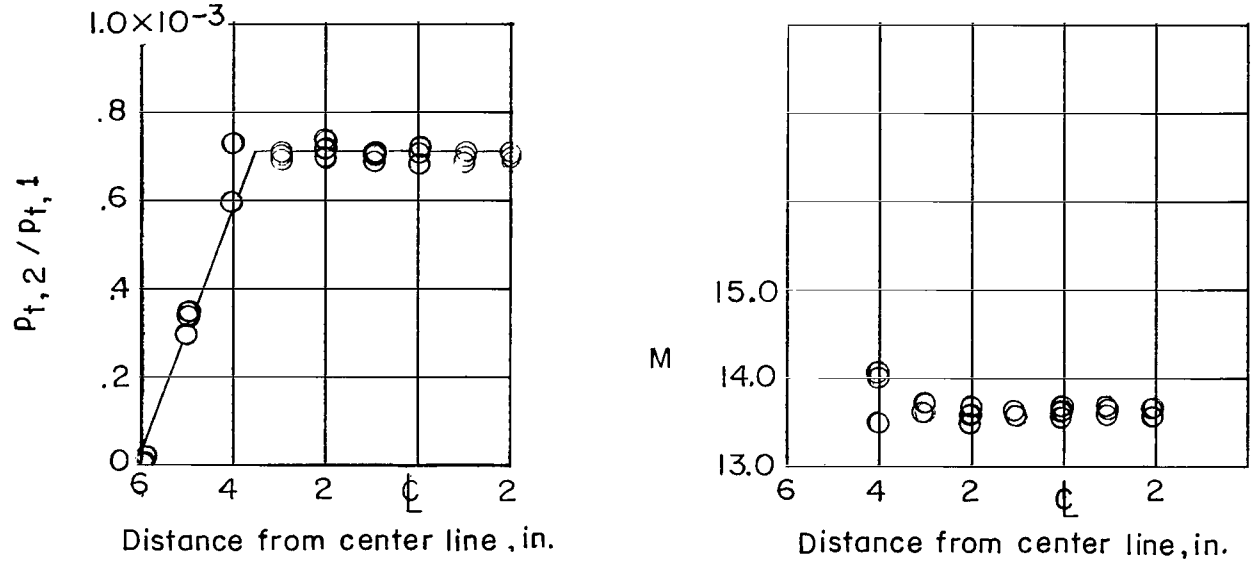

(a) $p_{t,1}$ = 615 psia.

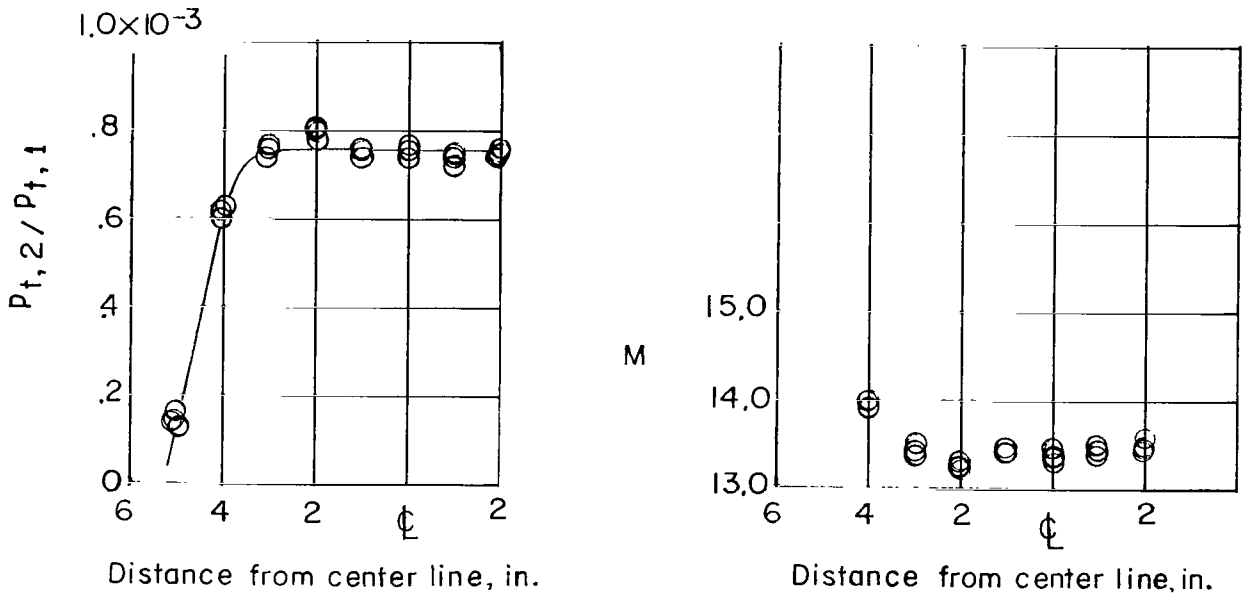

(b) $p_{t,1}$ = 315 psia.

Figure 7.- Lateral total-pressure surveys and Mach number distributions for several stagnation pressures at x = 2.3 inches. T_t = 3240° R.

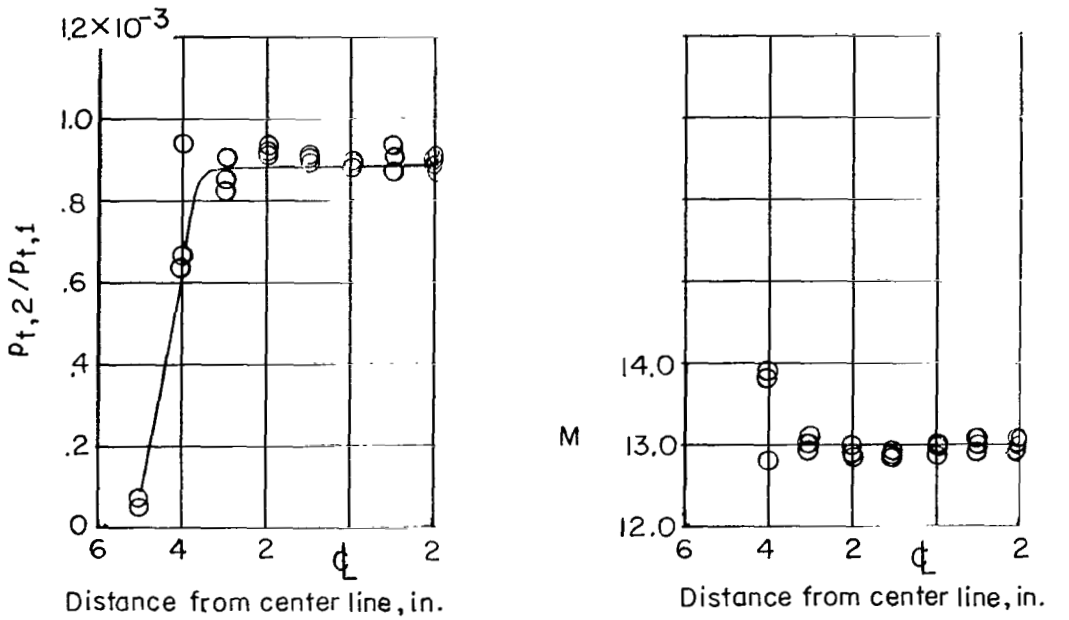

(c) $p_{t,1}$ = 115 psia.

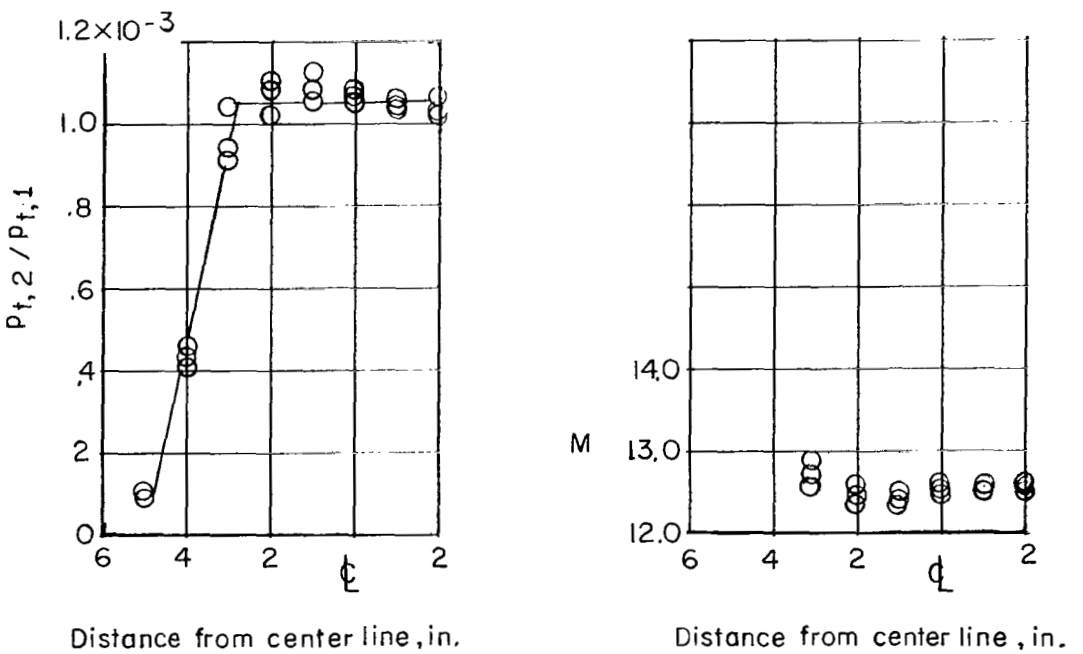

(d) $p_{t,1}$ = 65 psia.

Figure 7.- Concluded.

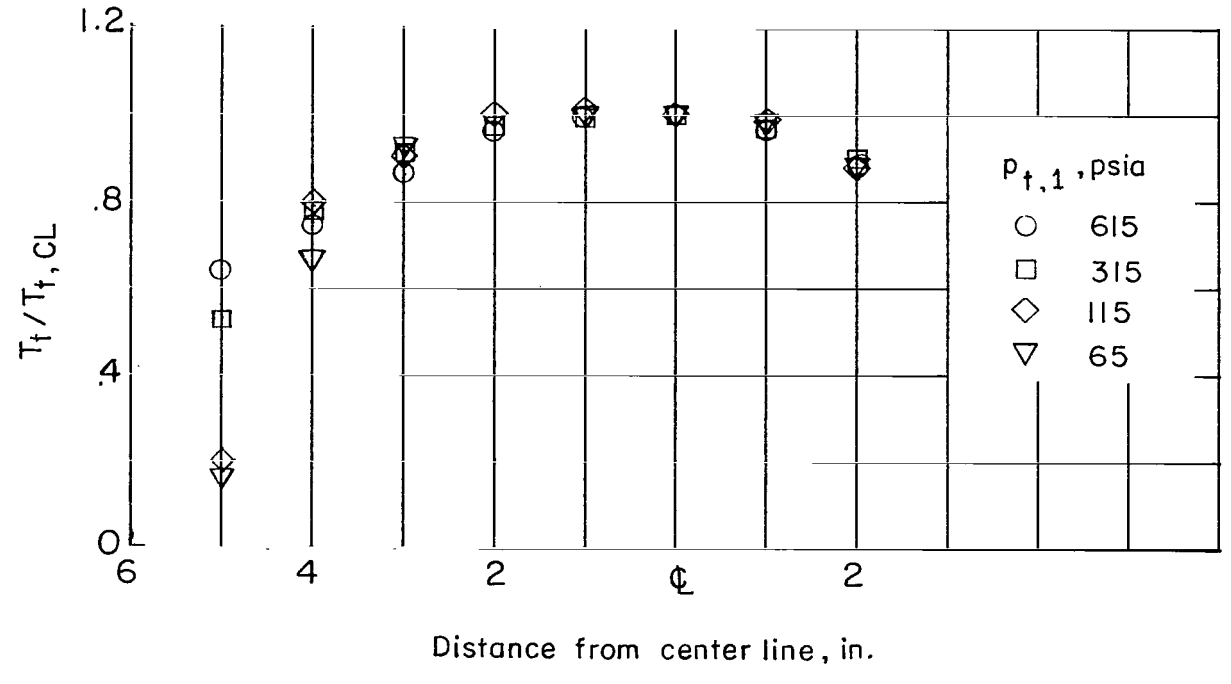

(a) Total temperature.

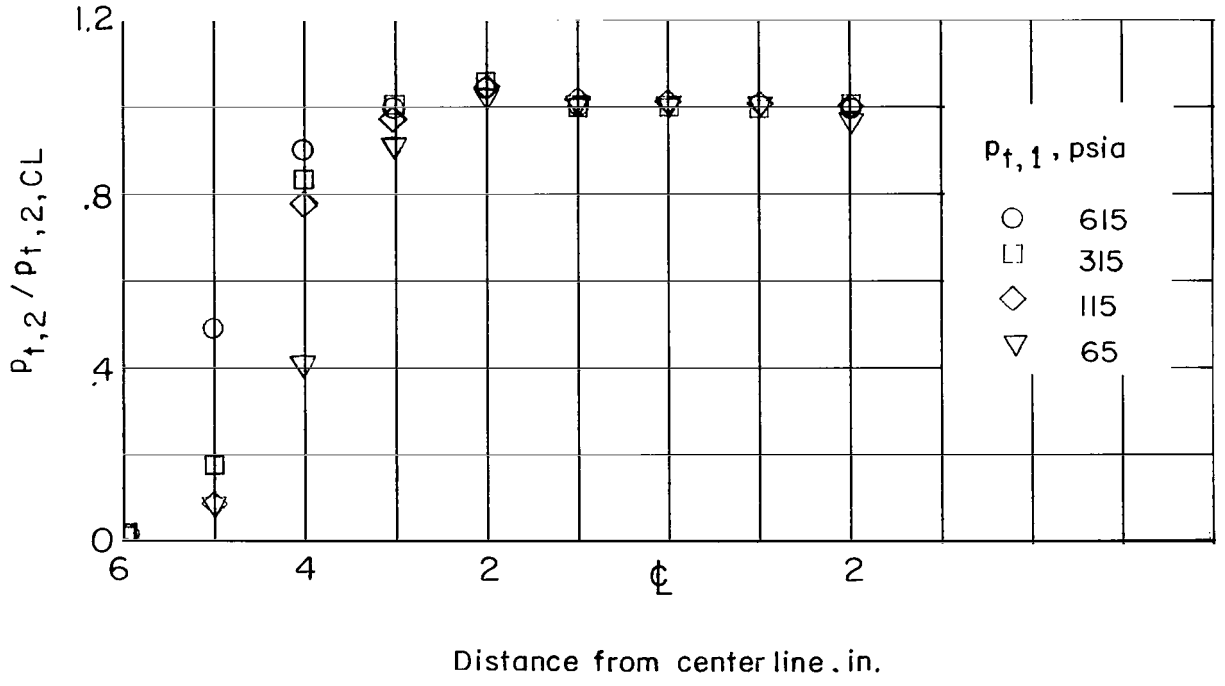

(b) Total pressure. T_t = 3240° R.

Figure 8.- Comparison of total pressure and temperature profiles at various stagnation pressures.

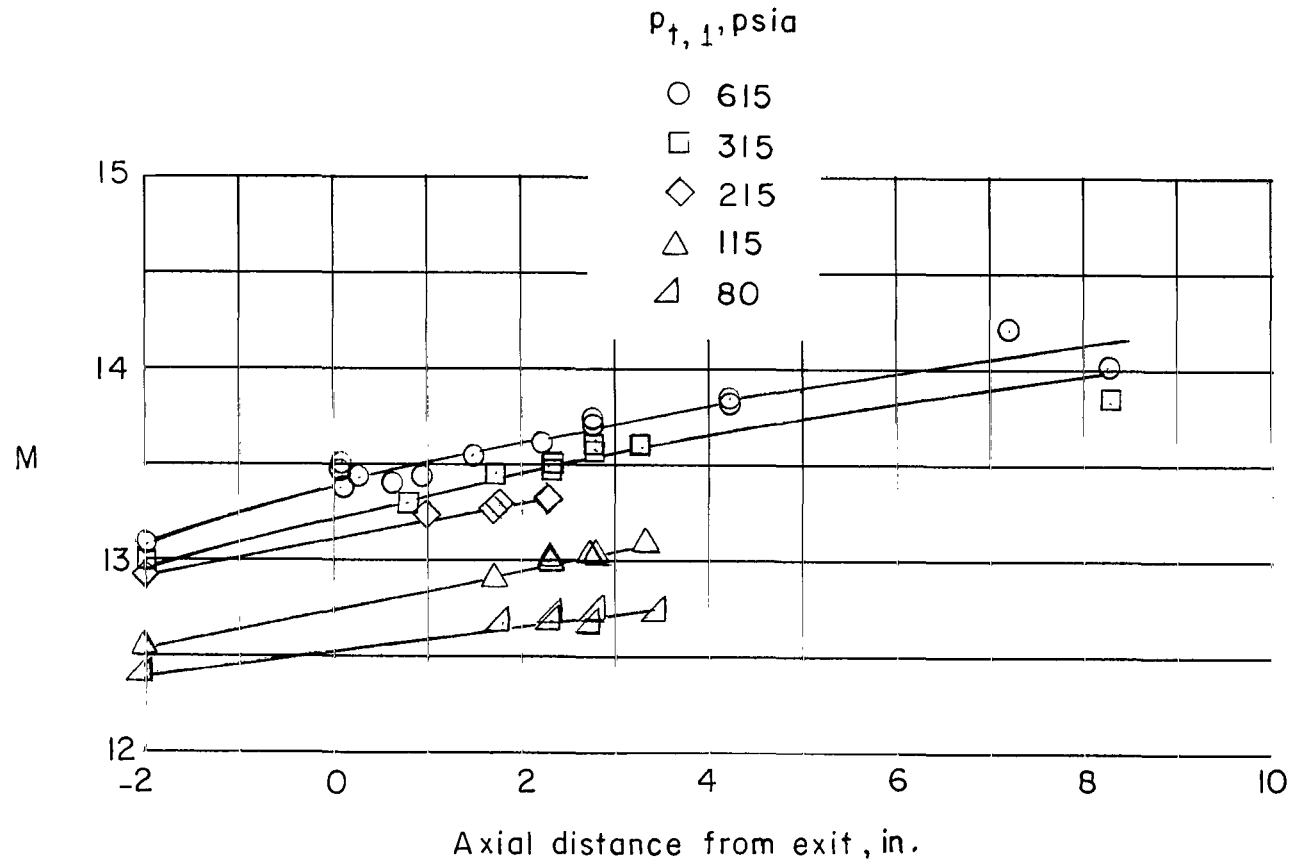

Figure 9.- Axial Mach number gradient from total-pressure surveys along center line of nozzle at various stagnation pressures.

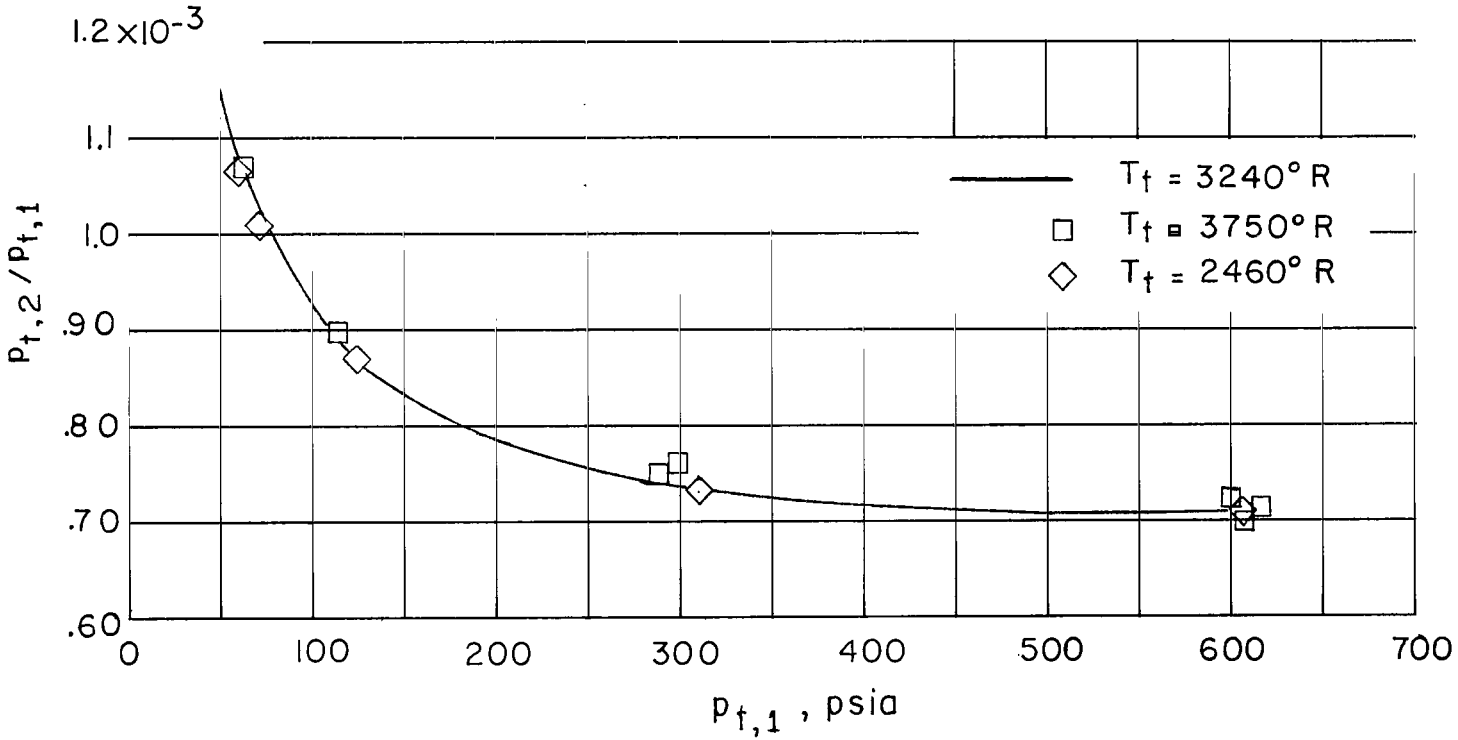

Figure 10.- Variation of $p_{t,2}/p_{t,1}$ on center line with stagnation pressure for several total temperatures.

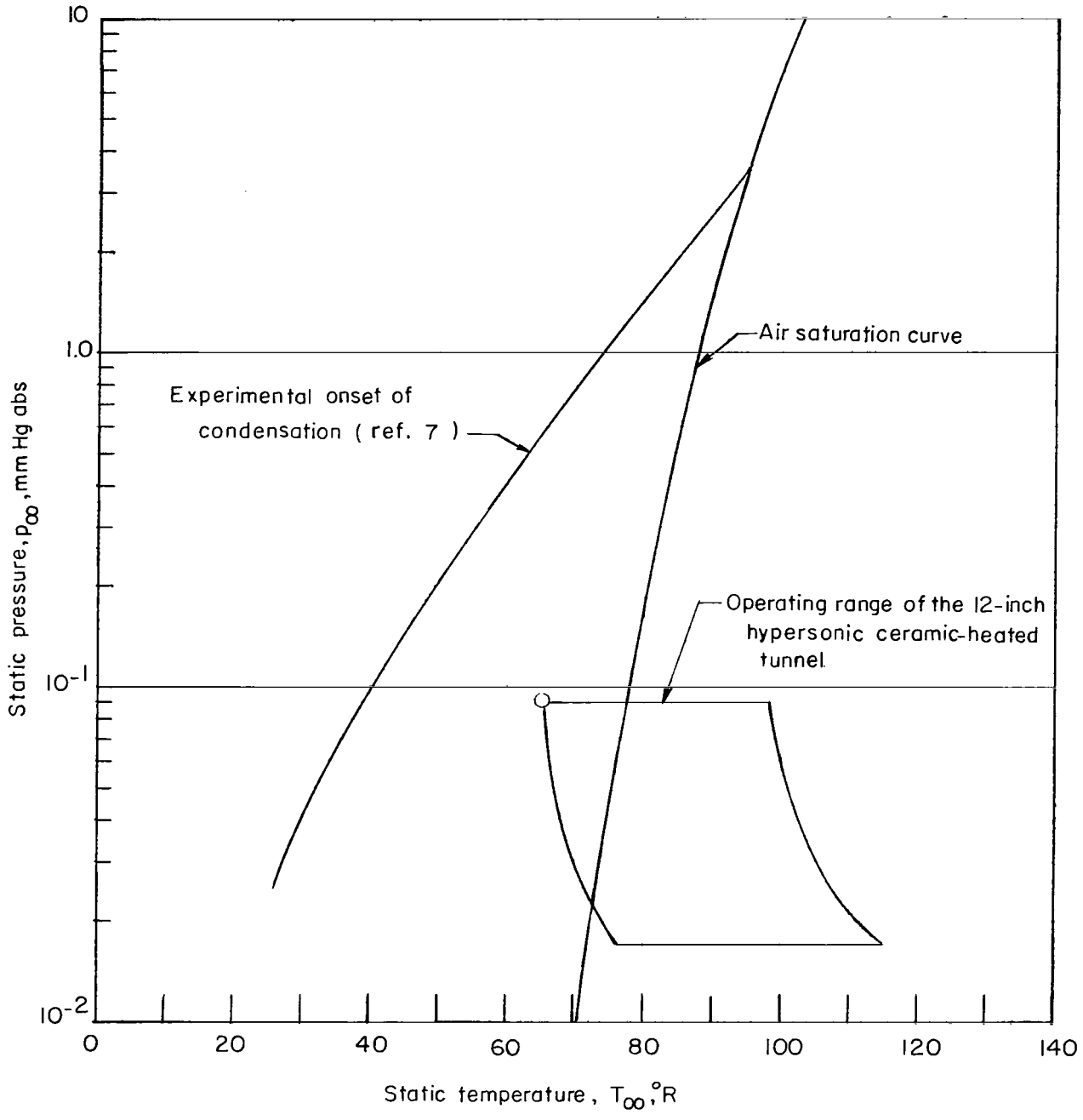

Figure 11.- Operating range of 12-inch hypersonic ceramic-heated tunnel in relation to air saturation curve and experimentally determined curve for onset of air condensation.

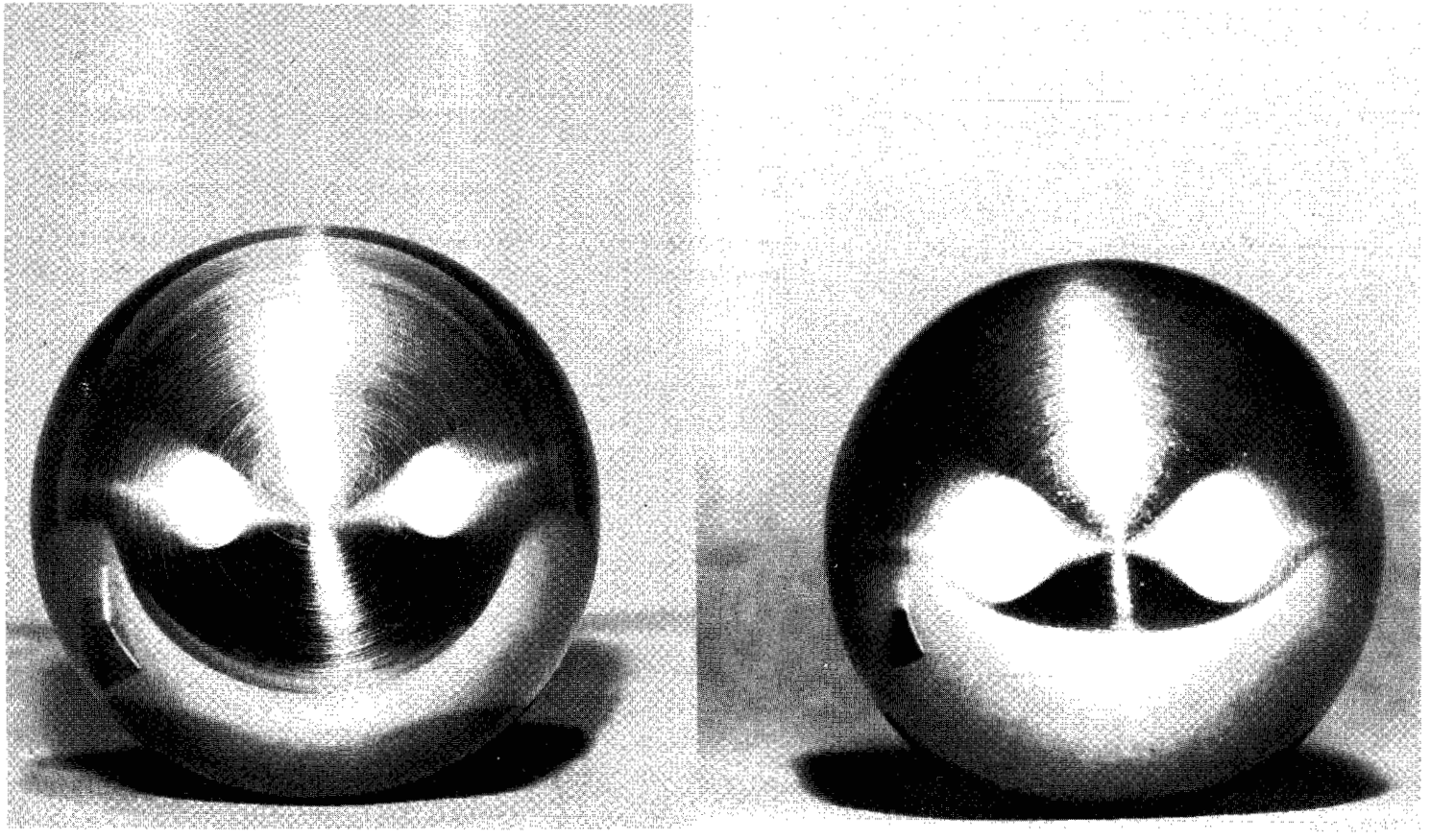

Before test

After test

Figure 12.- A $2\frac{1}{2}$- inch-diameter hemisphere cylinder before and after test. L-64-10212

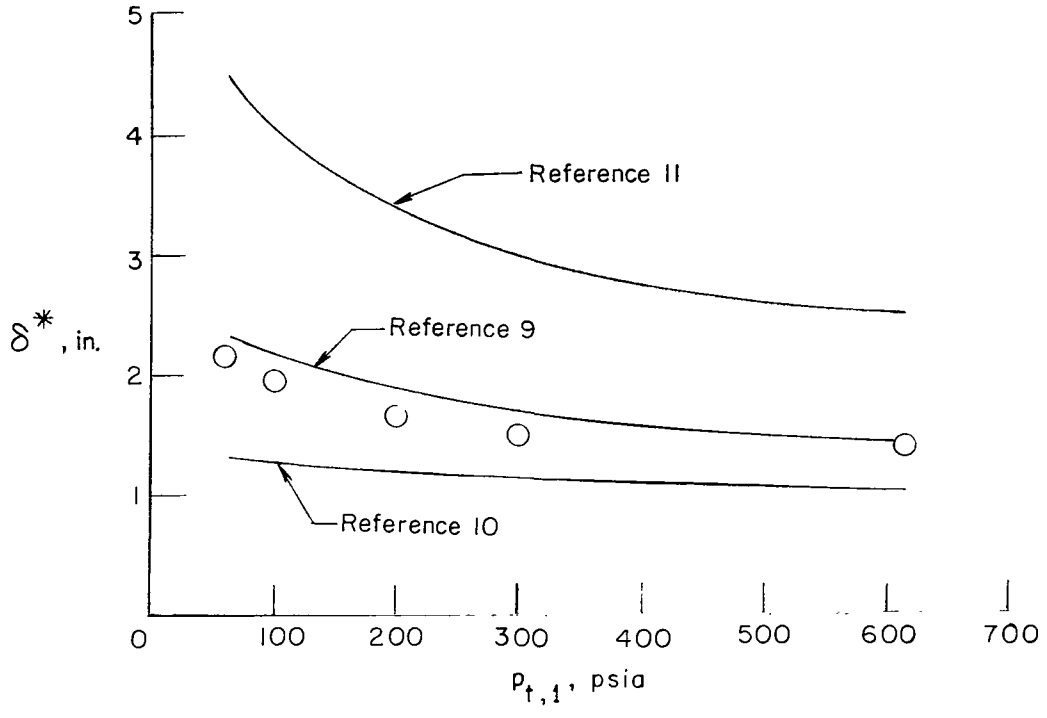

(a) Boundary-layer displacement thickness.

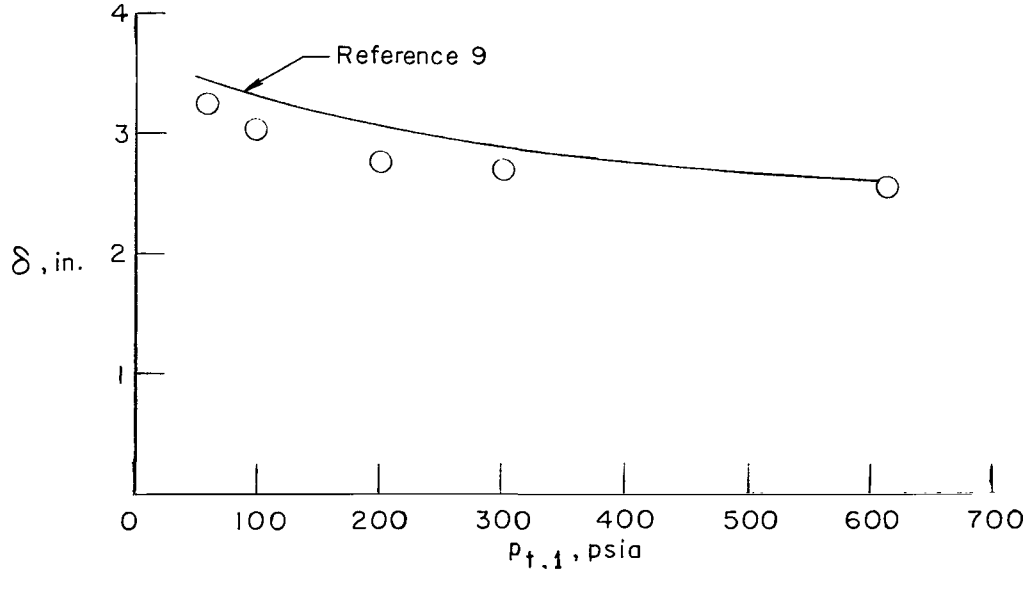

(b) Boundary-layer thickness.

Figure 13.- Variation of boundary-layer displacement thickness and boundary-layer thickness at nozzle exit with stagnation pressure. T_t = 3240° R.

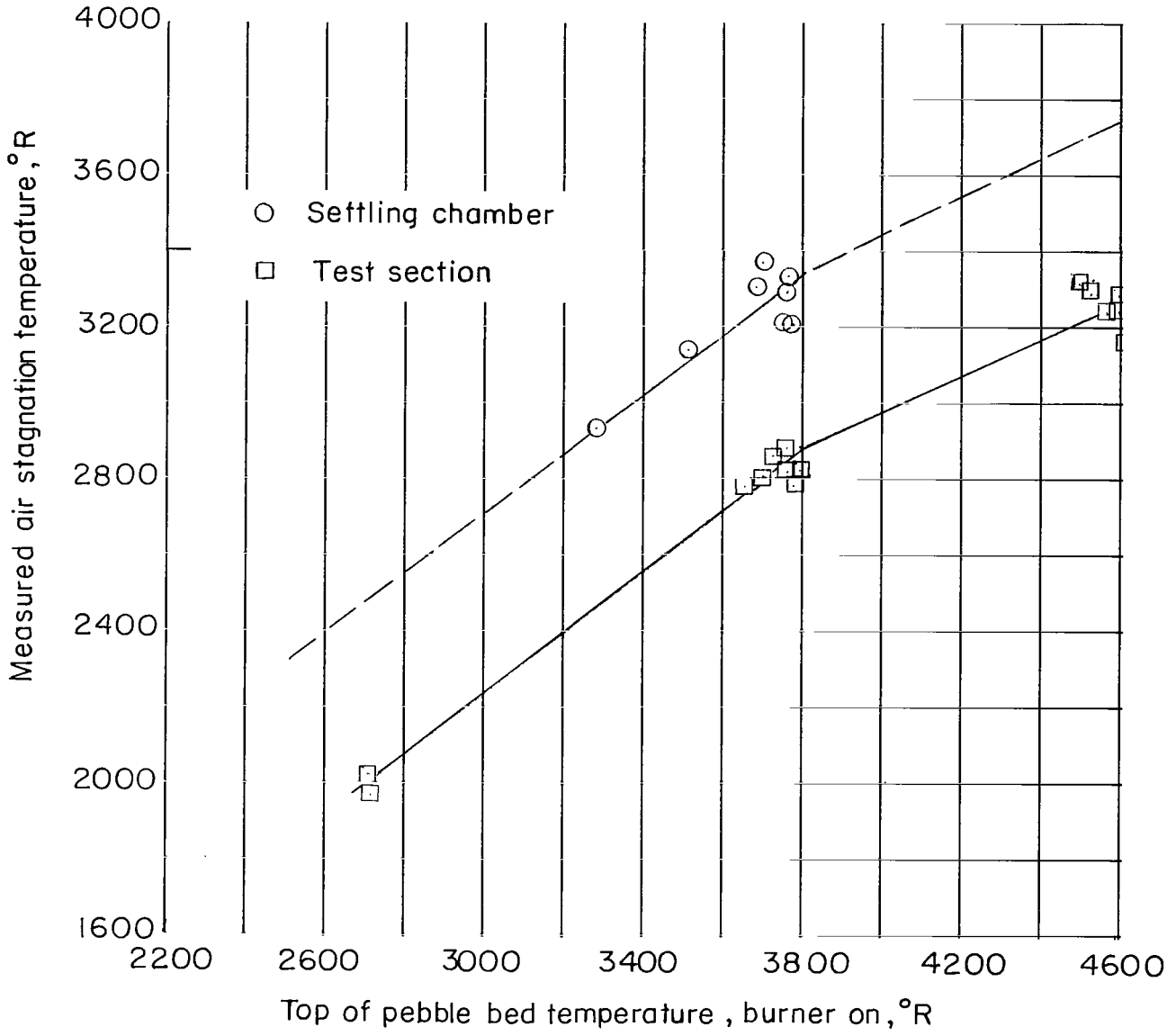

Figure 14.- Comparison of air stagnation temperature measured by settling chamber and test-section probes.

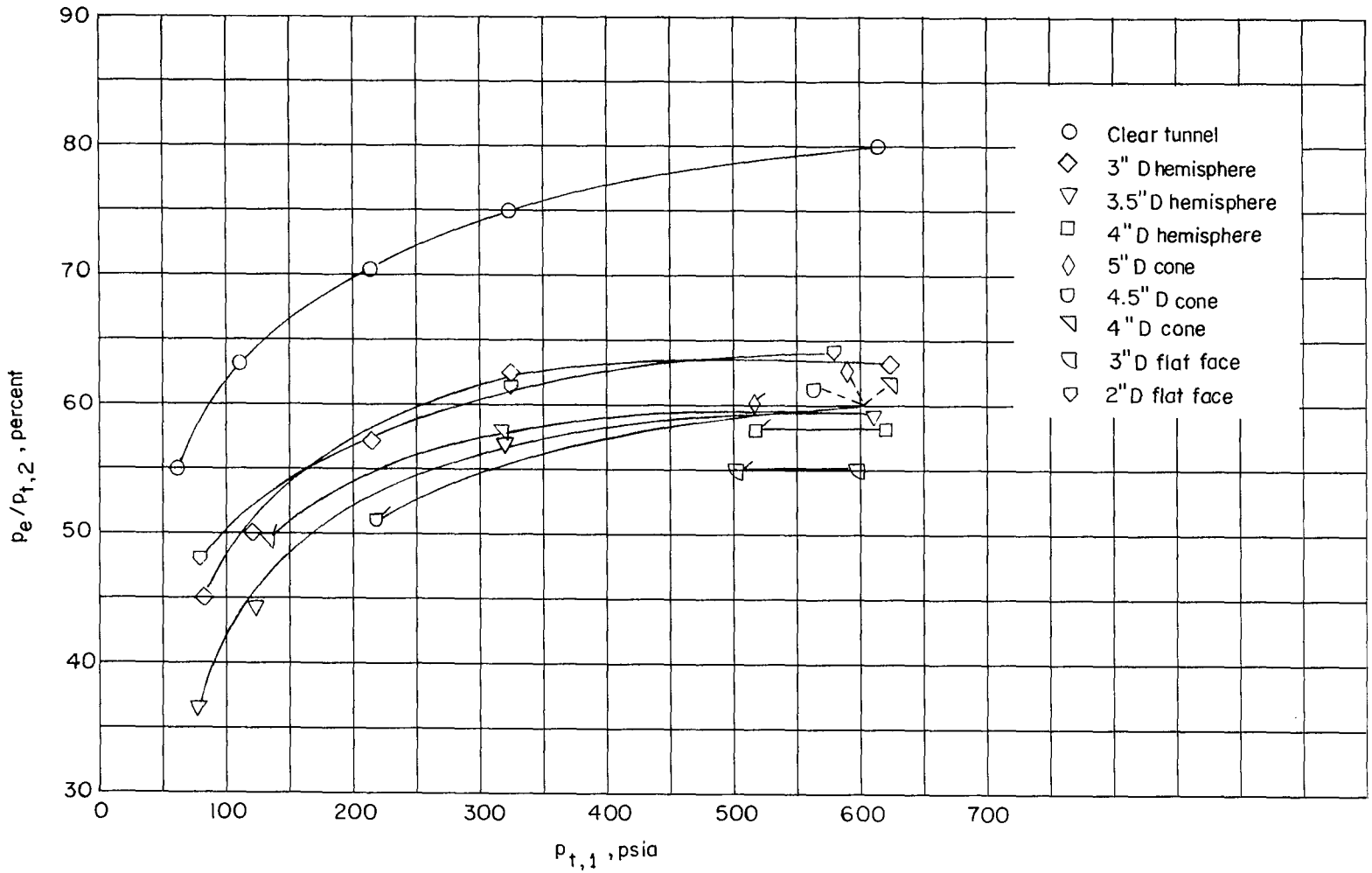

Figure 15.- Variation of diffuser pressure recovery over a range of stagnation pressure including effects of model blockage. Flagged symbols indicate lowest stagnation pressure at which model could be operated.

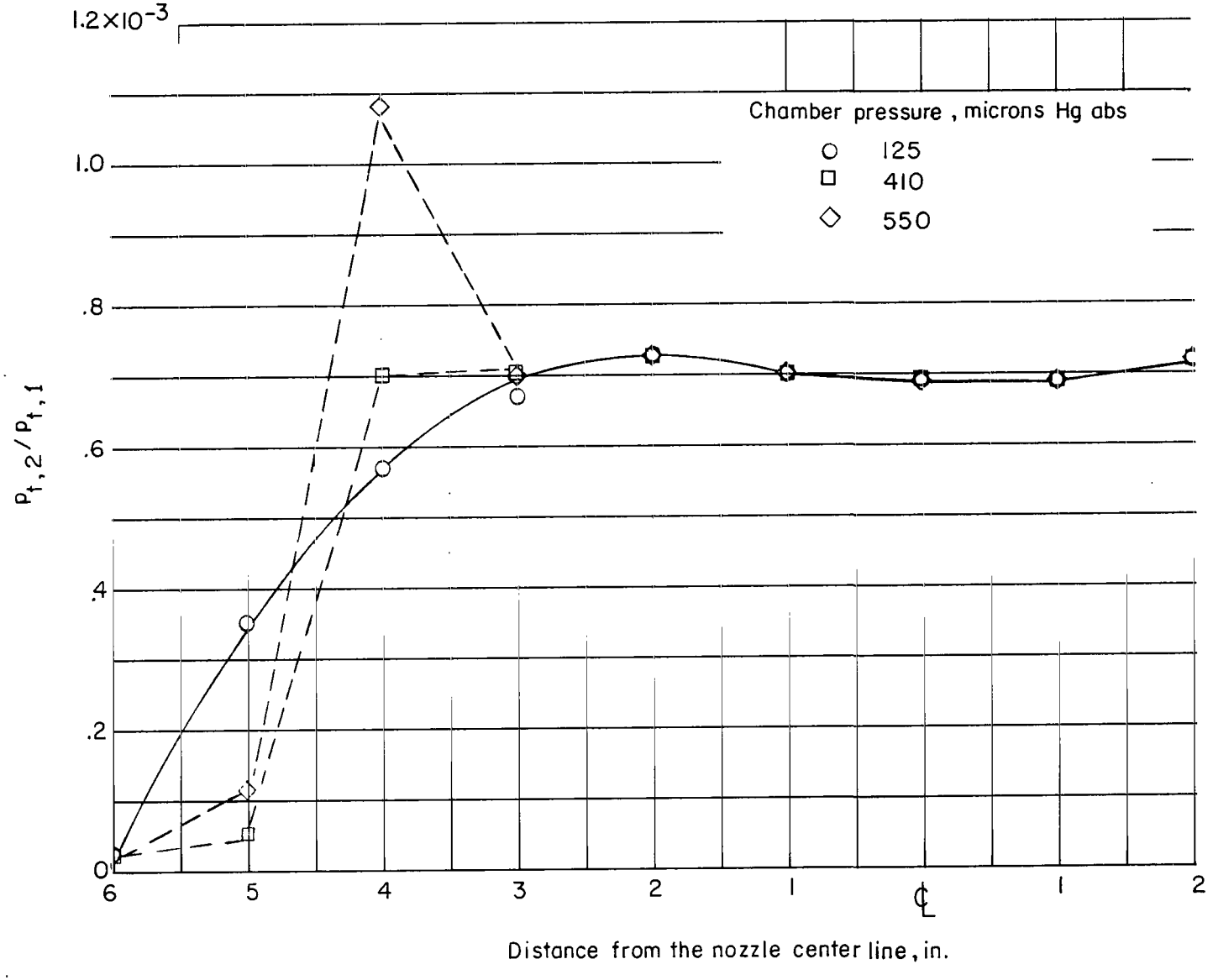

Figure 16.- Effect of chamber pressure on lateral pitot-pressure profile. x = 2.3 in; $p_{t,1}$ = 600 psia.

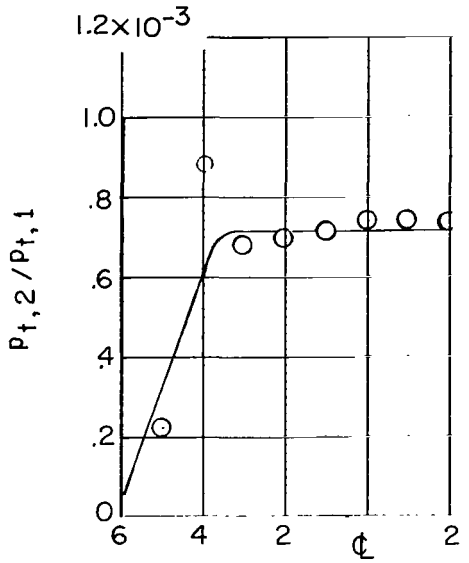

Distance from the center line, in.

(a) $p_{t,1}$ = 615 psia; $p_c/p_\infty \approx 4$.

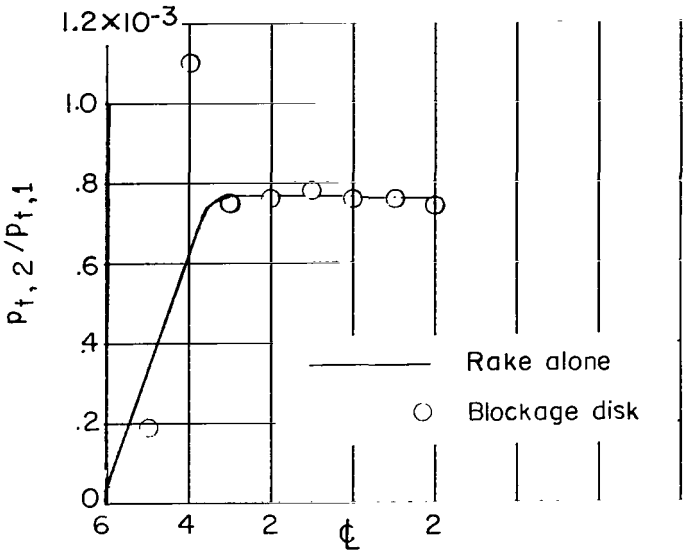

Distance from the center line, in.

(b) $p_{t,1}$ = 315 psia; $p_c/p_\infty \approx 4$.

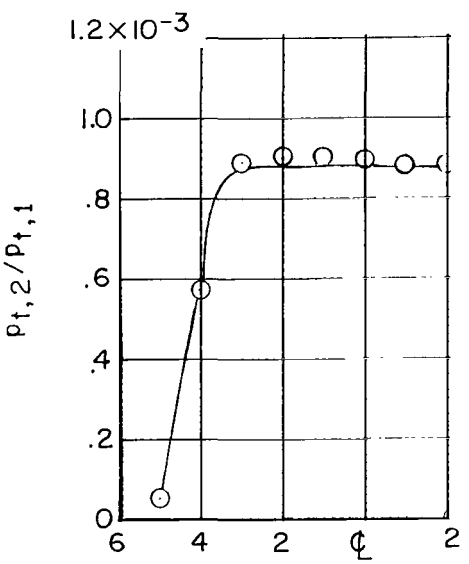

Distance from the center line, in.

(c) $p_{t,1}$ = 115 psia; $p_c/p_\infty \approx 4$.

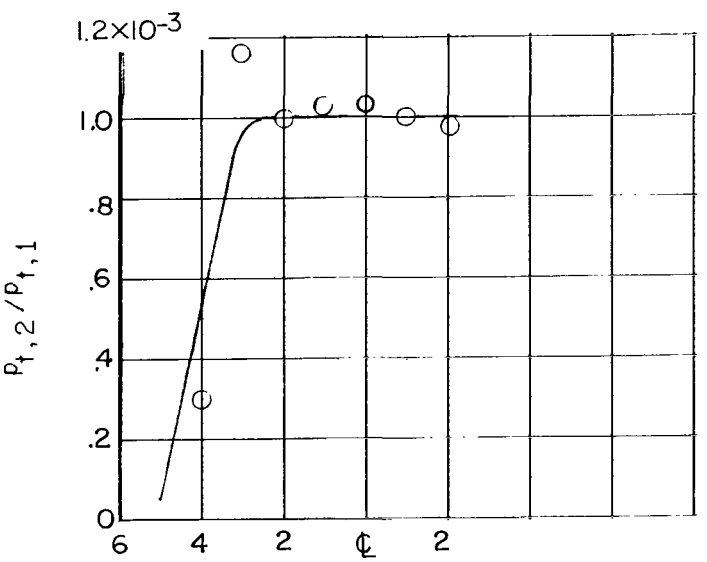

Distance from the center line, in.

(d) $p_{t,1}$ = 65 psia; $p_c/p_\infty \approx 5$.

Figure 17.- Effect of free-jet chamber pressure on lateral pitot-pressure profiles at various stagnation pressures for diffuser configuration 3. x = 2.3 in.

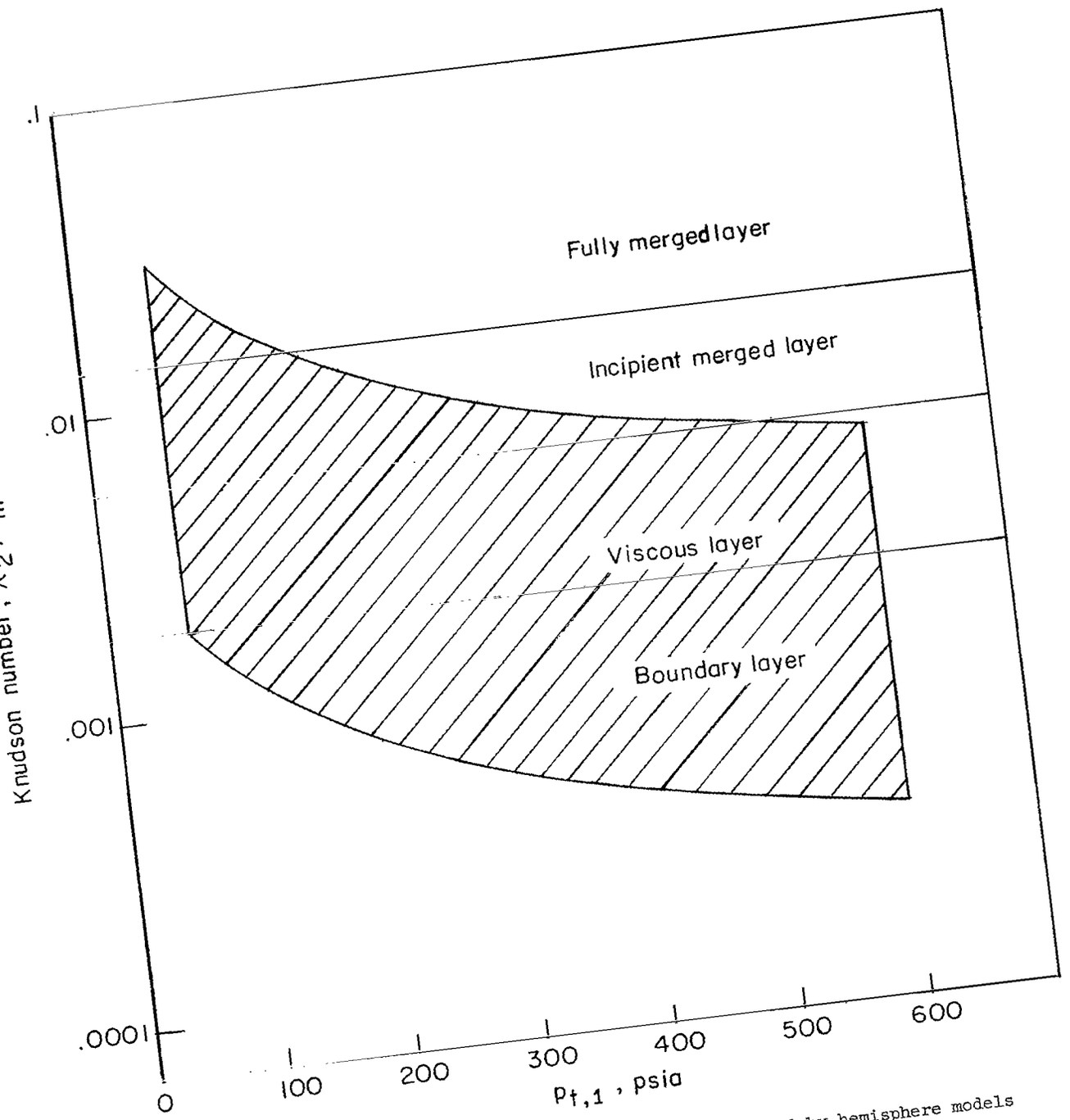

Figure 18.- Rarefied-gas regimes for blunt-nose bodies simulated by hemisphere models in the Langley 12-inch hypersonic ceramic-heated tunnel.

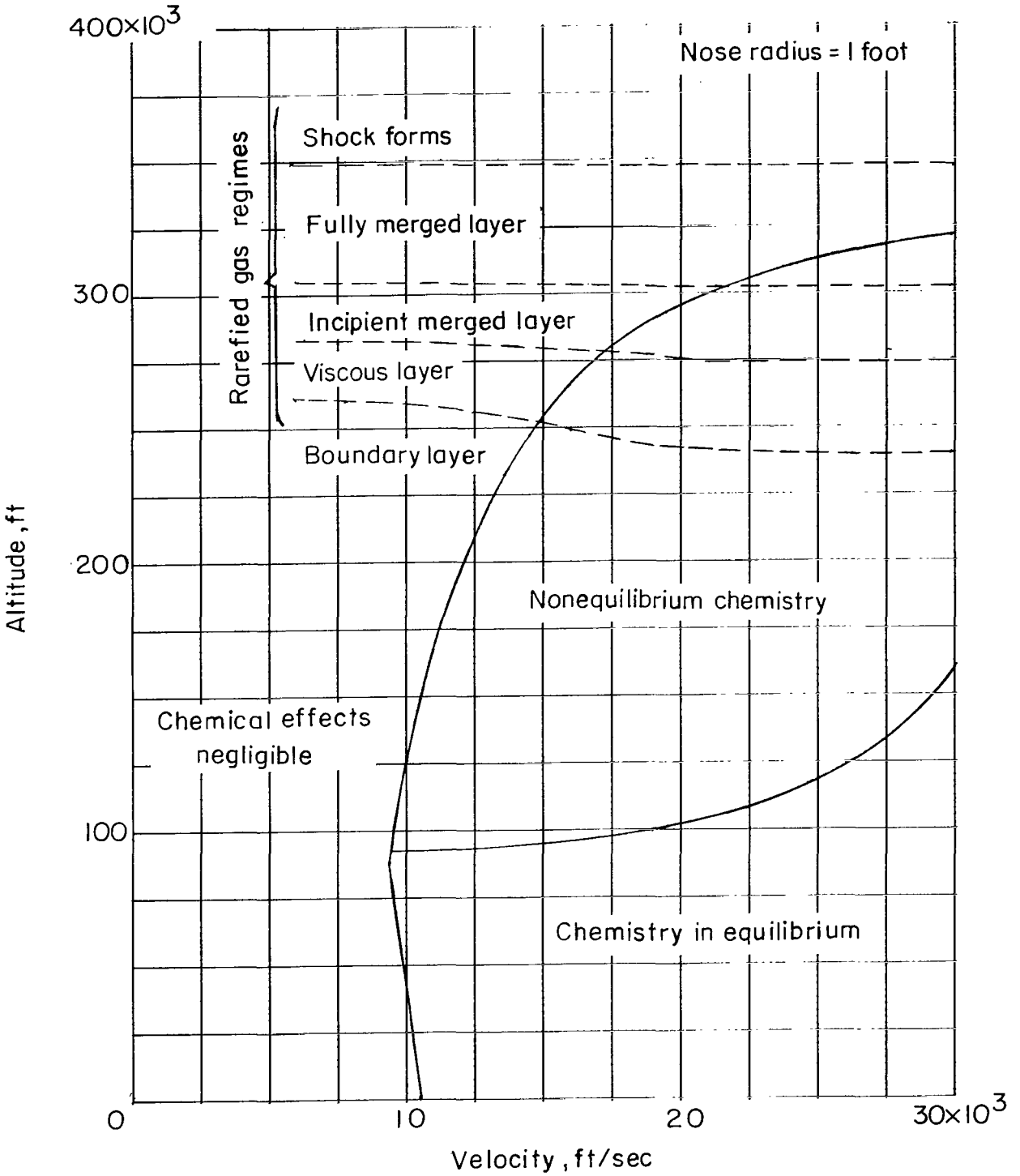

Figure 19.- Comparison of chemical kinetic and rarefied-gas regimes for flow with blunt-nose models. (From ref. 13.)

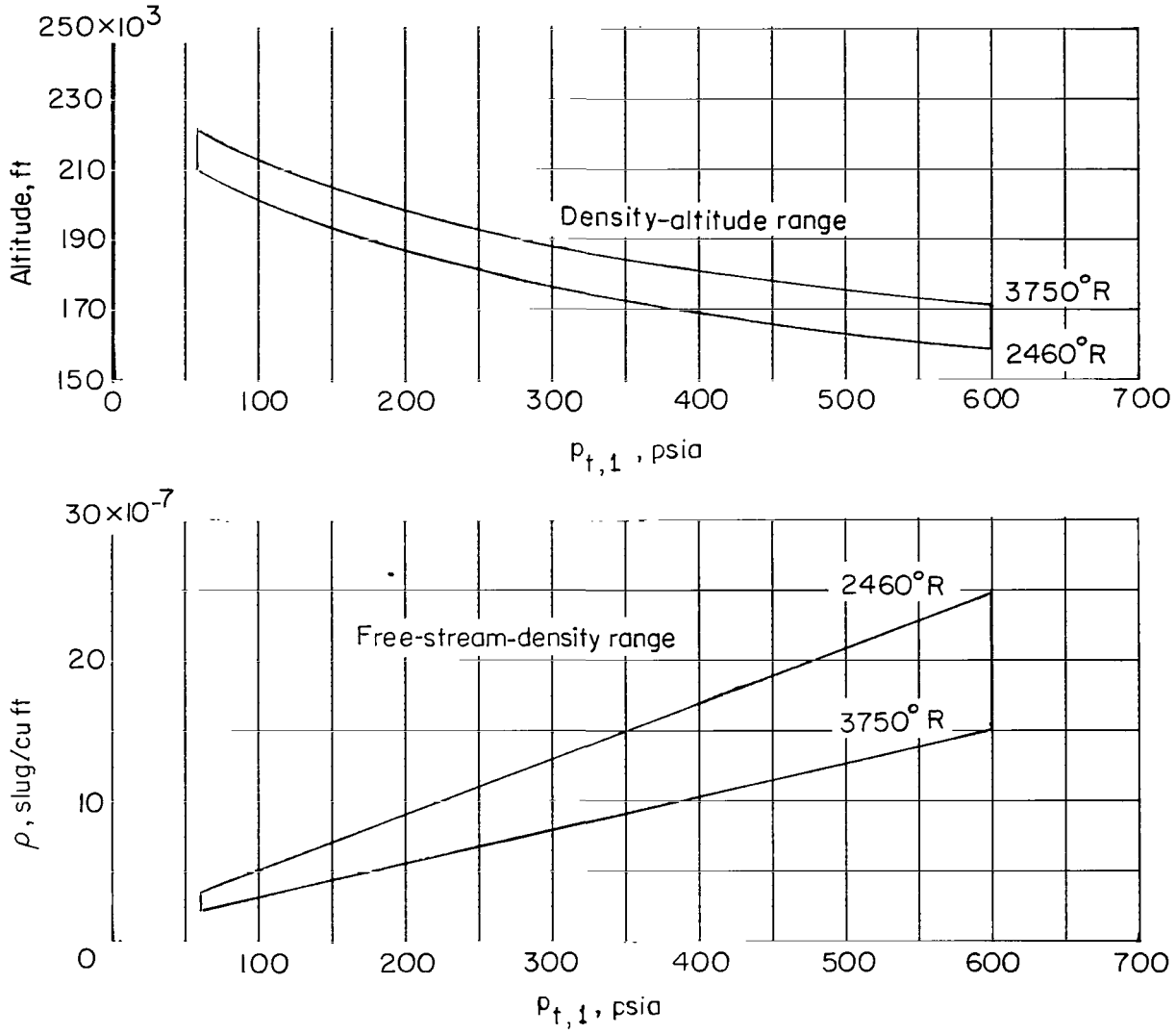

Figure 20.- Range of tunnel parameters.

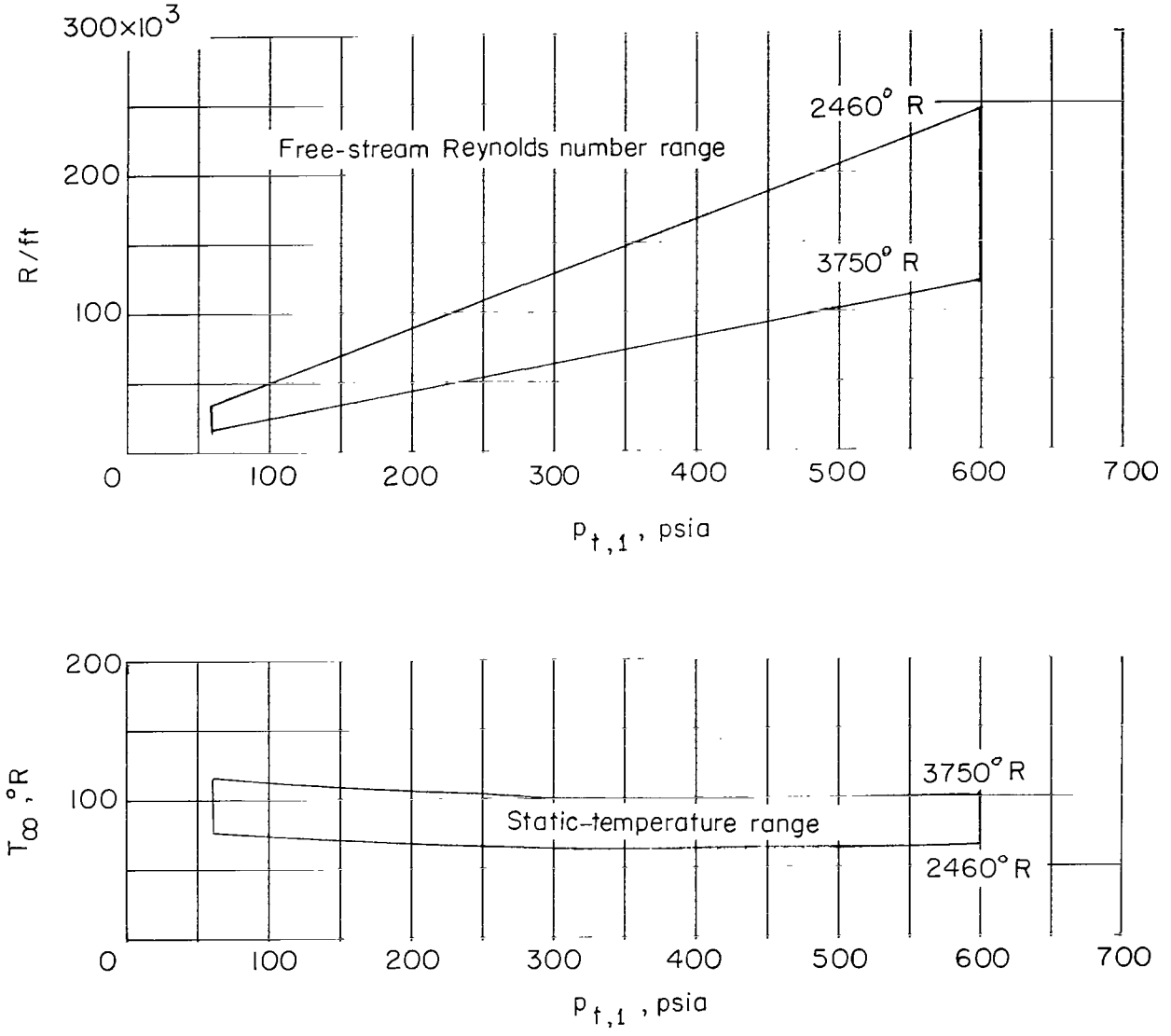

Figure 20.- Continued.

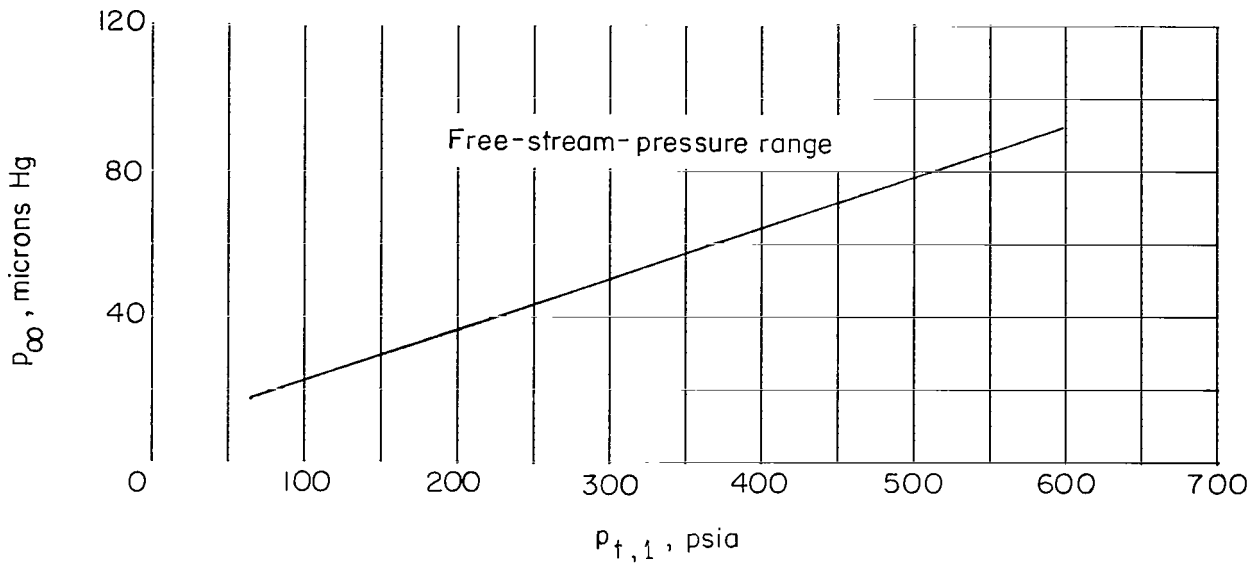

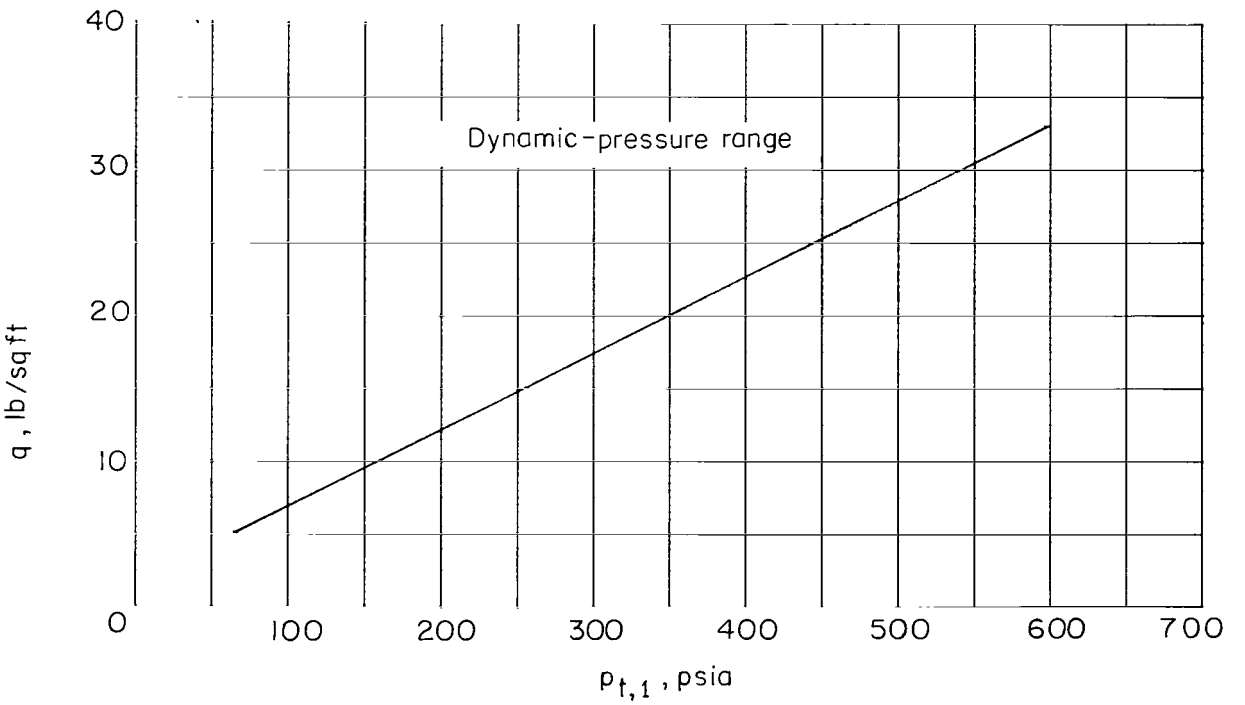

Figure 20.- Continued.

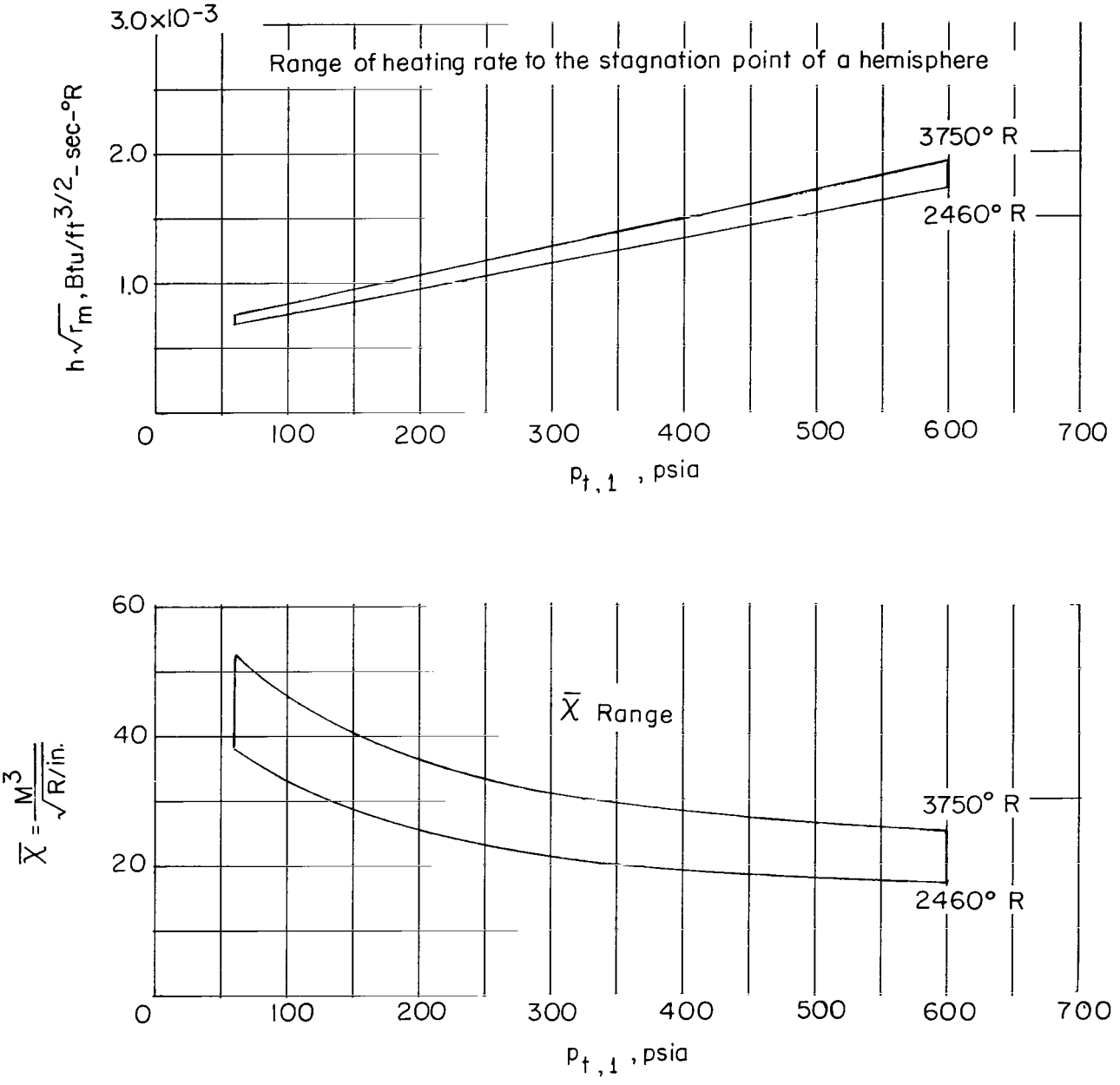

Figure 20.- Concluded.

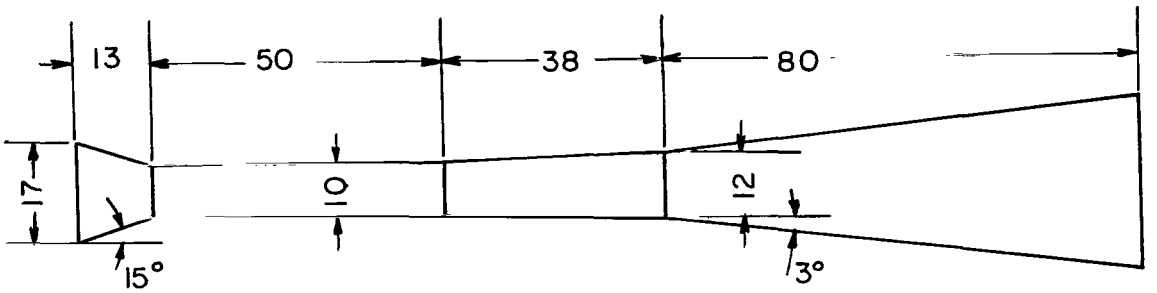

Configuration 1

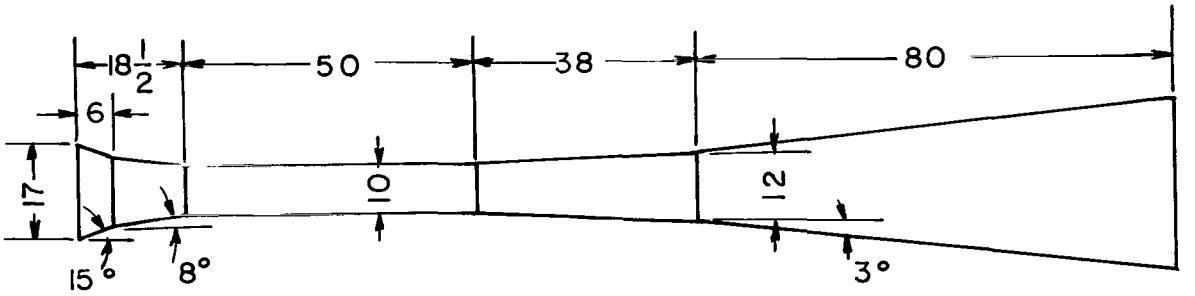

Configuration 2

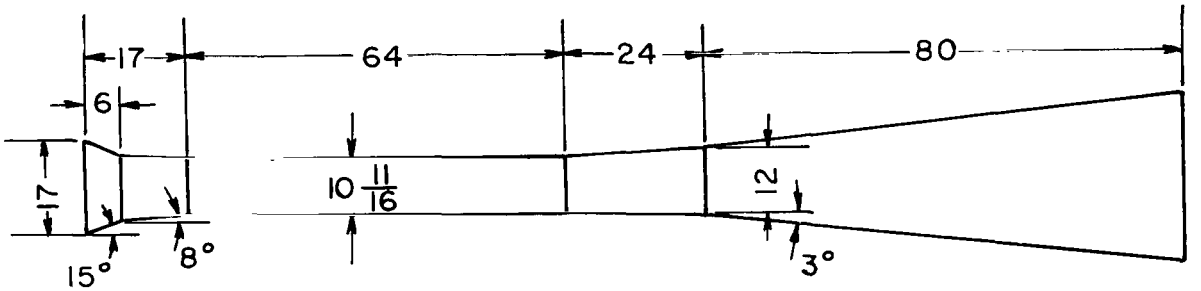

Configuration 3

Diffuser configuration	Free-jet length / Nozzle exit diam.	Second min. length / Second min. diam.	Second min. area / Nozzle exit area
1	1.14	5	0.69
2	.67	5	.69
3	.78	6	.79

Figure 21.- Diffuser configurations tested. All linear dimensions are in inches.

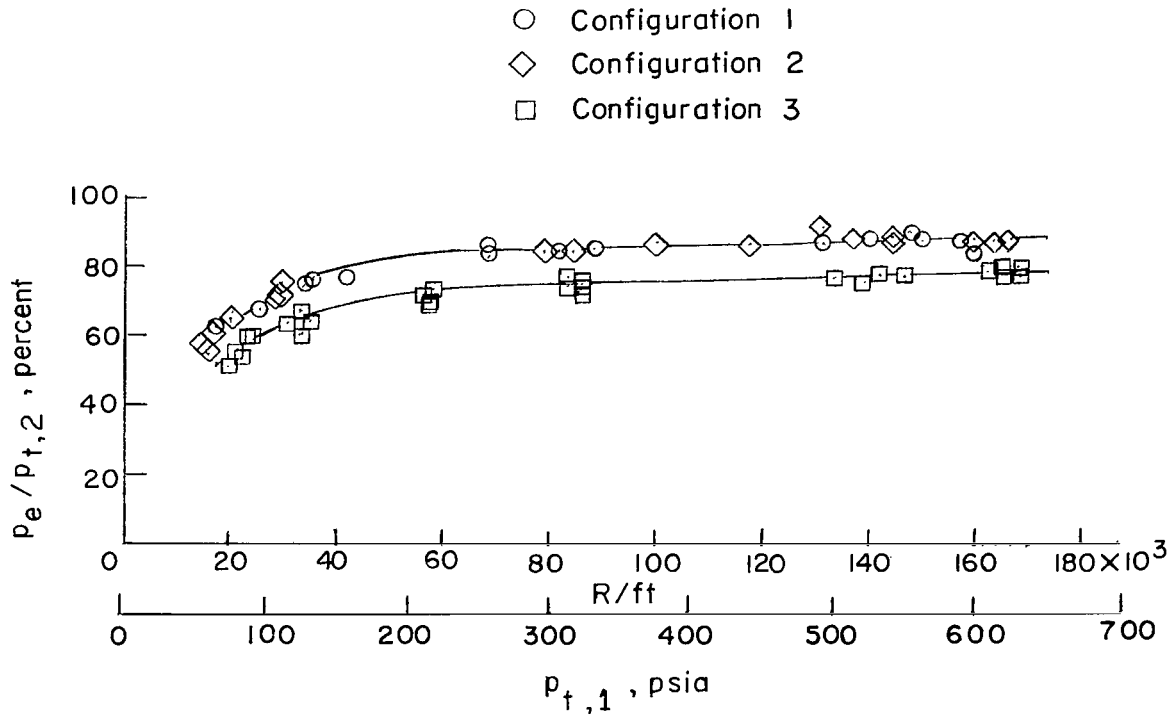

Figure 22.- Variation of clear-tunnel pressure recovery with free-stream Reynolds number per foot.

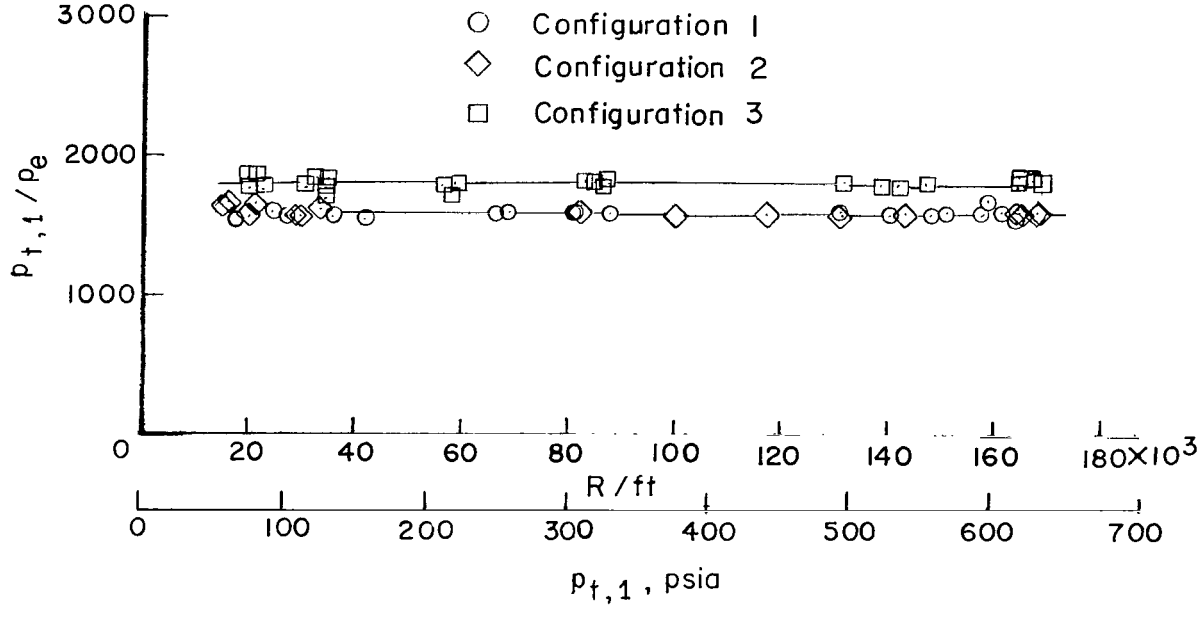

Figure 23.- Variation of pressure ratio required to maintain flow with free-stream Reynolds number per foot.

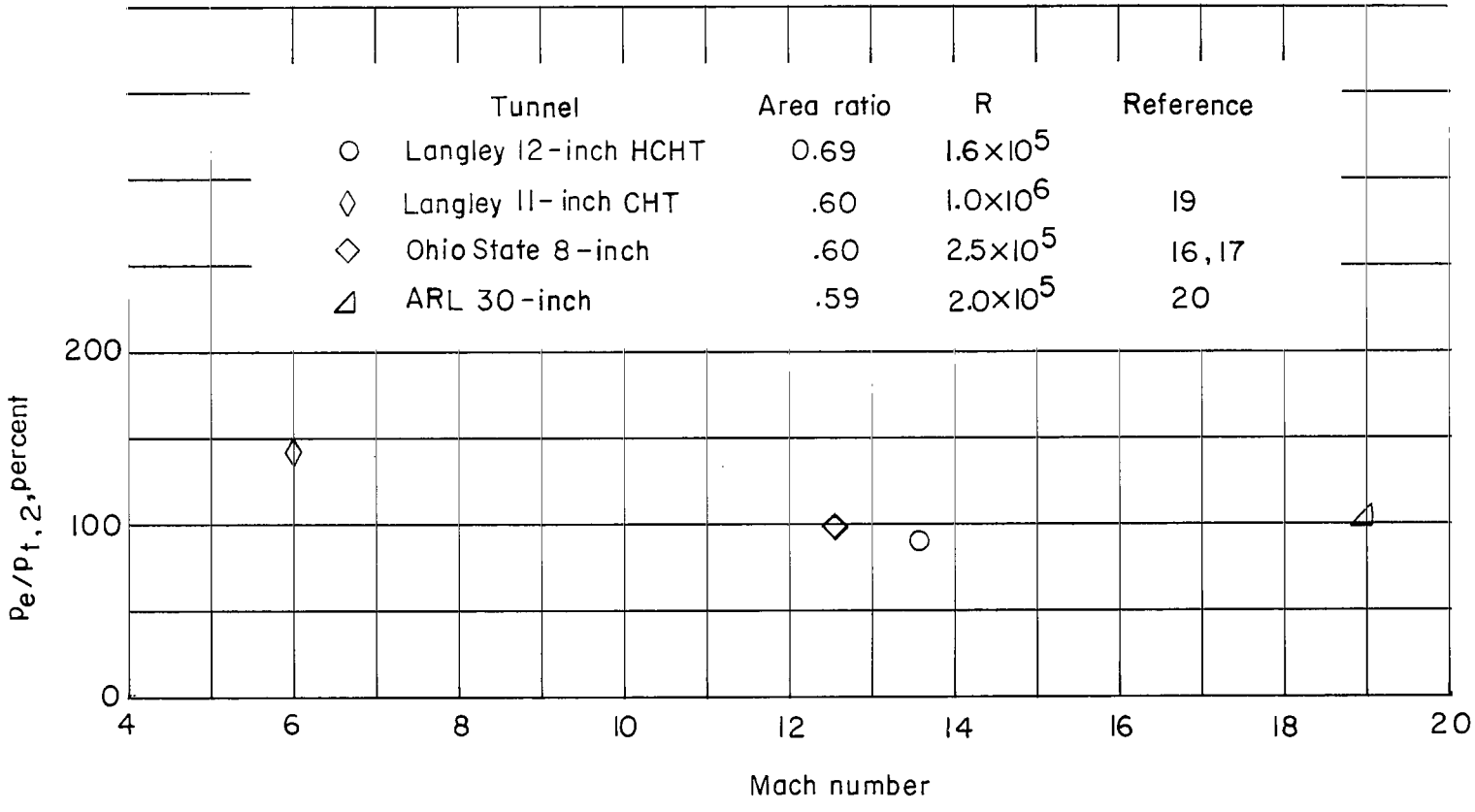

Figure 24.- Comparison of percent normal shock recovery for several free-jet wind tunnels over a range of Mach numbers.

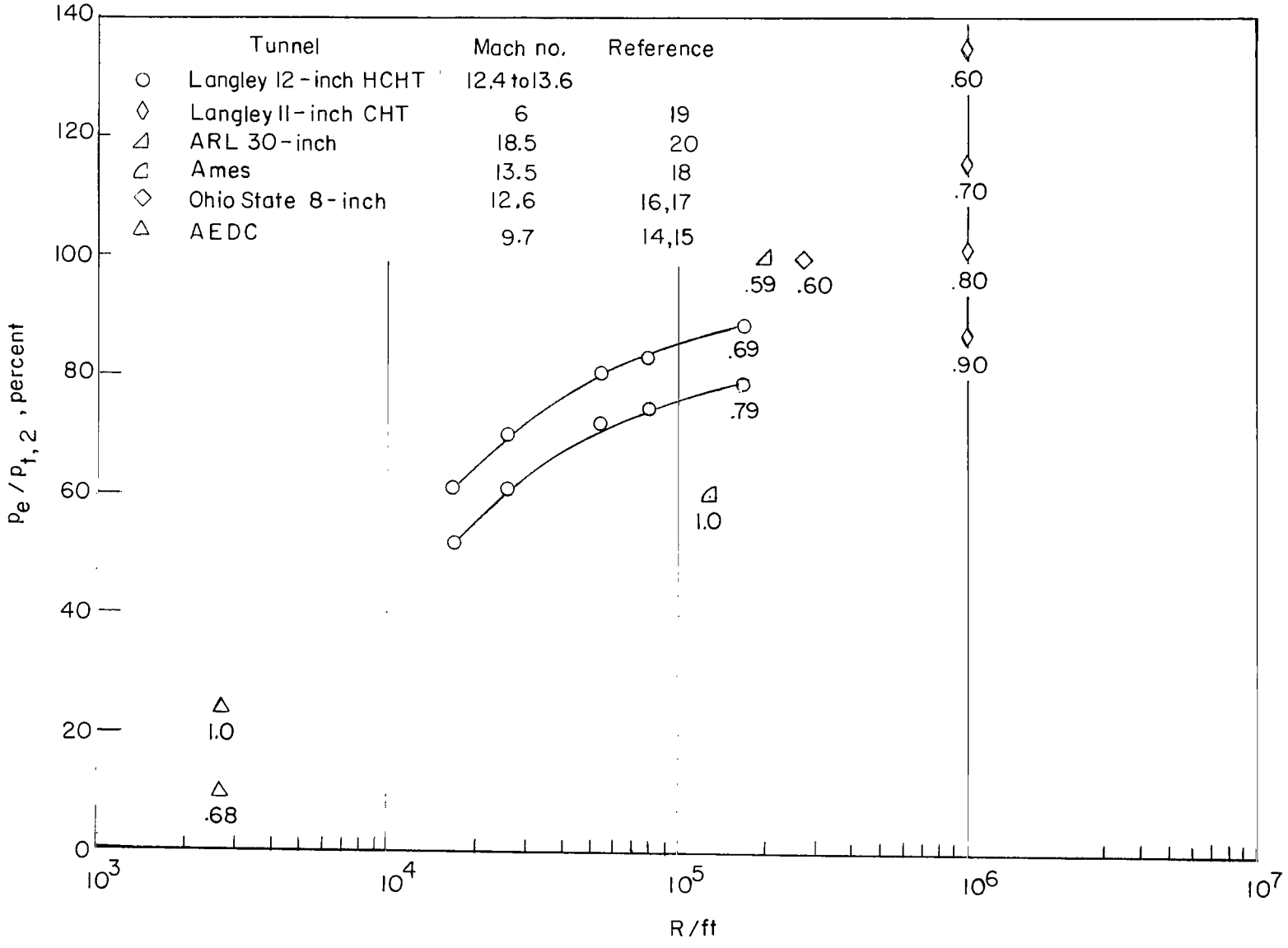

Figure 25.- Comparison of percent normal shock recovery for several free-jet wind tunnels over a range of Reynolds number. Number below data points indicates second minimum area ratio.

2/22/85

"The aeronautical and space activities of the United States shall be conducted so as to contribute . . . to the expansion of human knowledge of phenomena in the atmosphere and space. The Administration shall provide for the widest practicable and appropriate dissemination of information concerning its activities and the results thereof."

—NATIONAL AERONAUTICS AND SPACE ACT OF 1958

NASA SCIENTIFIC AND TECHNICAL PUBLICATIONS

TECHNICAL REPORTS: Scientific and technical information considered important, complete, and a lasting contribution to existing knowledge.

TECHNICAL NOTES: Information less broad in scope but nevertheless of importance as a contribution to existing knowledge.

TECHNICAL MEMORANDUMS: Information receiving limited distribution because of preliminary data, security classification, or other reasons.

CONTRACTOR REPORTS: Technical information generated in connection with a NASA contract or grant and released under NASA auspices.

TECHNICAL TRANSLATIONS: Information published in a foreign language considered to merit NASA distribution in English.

TECHNICAL REPRINTS: Information derived from NASA activities and initially published in the form of journal articles.

SPECIAL PUBLICATIONS: Information derived from or of value to NASA activities but not necessarily reporting the results of individual NASA-programmed scientific efforts. Publications include conference proceedings, monographs, data compilations, handbooks, sourcebooks, and special bibliographies.

Details on the availability of these publications may be obtained from:

SCIENTIFIC AND TECHNICAL INFORMATION DIVISION

NATIONAL AERONAUTICS AND SPACE ADMINISTRATION

Washington, D.C. 20546